# Electron–optical properties of atomic fields*

U. Fano and C. E. Theodosiou

*Department of Physics, The University of Chicago, Chicago, Illinois 60637*

J. L. Dehmer

*Argonne National Laboratory, Argonne, Illinois 60439*

We present a unified discussion and illustrations of the electron-optical aspects of electron penetration into, or escape from, the inner region of atoms. Both processes may focus or defocus the amplitudes of wavefunctions and shift their phases, as manifested in countless phenomena ranging from level shifts to $\beta$-decay rates. A background survey begins by discussing the Fermi-Segrè formula for hyperfine splittings and emphasizes the interplay of hydrogenic and WKB approximations. The Phase-Amplitude Method, which determines amplitude ratios and phase shifts directly, proves useful for interpreting the systematics of these parameters along the Periodic System. We present results of survey calculations, carried through the Periodic System using Hartree–Slater potential fields, of: (a) $\alpha_l(0)/\alpha_l(\infty)$, the ratio of the wavefunction's amplitude at $r=0$ to that outside the atom; (b) $\delta_l(E=0)$ and $d\delta_l/dE|_{E=0}$, the phase shift and its energy derivative at $E=0$; and (c) the changes in $\delta_l(E=0)$ and $\alpha_l(0)/\alpha_l(\infty)$ induced by either a unit perturbation localized near $r=0$ or a relativistic correction. Thus we provide a broad mapping of certain fundamental parameters based on rather crude but realistic calculations. These results are meant to serve as a bench mark in surveying problems and in checking new results, while standard methods are preferable for working out specific applications accurately.

## CONTENTS

| | | |
|---|---|---|
| I. | Introduction | 49 |
| II. | Background | 50 |
| III. | The Model Potential | 51 |
| IV. | The Phase-Amplitude Method (PAM) | 53 |
| V. | The WKB Approximation for Atomic Fields | 55 |
| VI. | $Z$-Dependence of the Amplitude Ratio $\alpha_l(0)/\alpha_l(\infty)$ | 56 |
| | A. Spin-orbit coupling | 58 |
| | B. Hyperfine interaction and other inner-shell phenomena | 60 |
| VII. | $Z$-Dependence of $\delta_l$ and $d\delta_l/dE$ at $E=0$ | 61 |
| VIII. | Response of $\alpha_l$ and $\delta_l$ to Perturbations Localized Near the Nucleus | 63 |
| | A. Delta-function perturbation | 64 |
| | B. The relativity perturbation | 65 |
| IX. | Concluding remarks | 66 |
| Acknowledgment | | 67 |
| References | | 67 |

## I. INTRODUCTION

A broad class of atomic properties depends on the deep penetration of electrons into the region near the nucleus. This class includes the fine and hyperfine structure of atomic levels and their shifts due to relativistic dynamics prevailing near the nucleus. Closely related are the effects of spin–orbit coupling and of relativistic dynamics upon the scattering of slow electrons by atoms or ions. All these effects are proportional to the squared amplitude of an electron's wave function near the nucleus, which in turn depends on the normalization of this function, and therefore on the ratio of its amplitudes in the limits of $r\to 0$ and $r\to\infty$.

Another important class of phenomena depends on the same ratio of wave function amplitudes, namely, the phenomena involving the escape of electrons released at or near a nucleus. This class includes $\beta$-decay, internal conversion, and the photoionization and Auger effect of inner shells. The probability of each of these processes is proportional to the squared amplitude of an electron's wave function at or near a nucleus, for a wave function normalized "per unit energy," i.e., with an amplitude standardized outside the atom. Bremsstrahlung and pair production depend on the product of two such squared amplitudes, for the initial and final states of a particle or for particle and antiparticle states, respectively, when the transitions take place near a nucleus.

The ratio of wave function amplitudes in the outer and inner reaches of the atom depends, of course, on the solution of the radial wave equation and thus on the atomic potential field prevailing throughout the range of intermediate distances from the nucleus. Variations of the potential field from one atom to another enhance or depress this amplitude ratio systematically along the Periodic System. Since the atomic field can so modify the amplitude of the electron's wave function, and hence the electron density, we have chosen to liken it to an electron–optical lens. This nomenclature is unorthodox in this context, but we feel it conveys an important aspect of the processes of electron penetration into, or escape from, an inner region of an atom.

This amplitude ratio is conjugate—in a quantum mechanical sense—to the phase shift which characterizes the elastic scattering of a free electron by an atomic or ionic field. The phase shifts of an electron–ion collision are in turn equivalent, when extrapolated to negative energy, to the quantum defects which determine the optical energy levels of a neutral atom in a single-electron model. The phase shifts and quantum defects are themselves electron–optical parameters of the atomic field, whose systematics are of obvious interest and have been studied occasionally in the past (Hellmig 1935; Griffin *et al.*, 1969; Manson 1969). The connection between the phase shifts and amplitude ratios belongs to the broad class of dispersion relations and will be discussed briefly in Sec. IV.

This article presents an overview of the electron–optical problem thus outlined and a set of illustrative data.

*Work supported by U. S. Energy Research and Development Administration, in part through Contract No. COO-1674-107.

The data show a smooth average dependence of amplitude ratios on the atomic number, modulated by striking effects of the progressive filling of outer shells. Paradoxically, our subject appears to have drawn little attention just because the calculation of a radial wave function for any specific problem amounts today to a rather trivial numerical exercise. Within the range of problems we consider, the exercise must have been carried out countless times as the need arose. On the other hand, directing attention to the general aspects of the problem and to qualitative and semiquantitative aspects of its solution should serve as a valuable bench mark in surveying problems and in checking results.

Early studies, particularly of fine and hyperfine structure in the 20's and 30's, did concern themselves with finding general formulas to represent the dependence of these properties on the atomic number, but later developments were scarce. Among these is a recent calculation of rates of slow-meson capture in the context of the Thomas–Fermi model (Leon and Seki, 1974). This model, however, apart from its well-known deficiencies in the extreme regions—both at the atomic surface and near the nucleus—does not incorporate the dependence on the shell structure. This dependence does manifest itself strikingly in the experimental data on meson capture (Wiegand 1969; Wiegand and Godfrey, 1973), whose connection with the variation of atomic radii along the Periodic System was subsequently pointed out by Condo (1974).

In fact, the studies reported in this article originate from the availability of extensive data on atomic potentials (Herman and Skillman, 1963) calculated by the Hartree–Slater (HS) model which incorporates the shell structure. A mapping of these potential data facilitated the survey of several properties, particularly of the effects of centrifugal potentials which depend critically on the radii of atoms (Rau and Fano, 1968, Fig. 1). Later on, with the intent of displaying the relationship between the potential field and the parameters of interest, we have been solving the Schrödinger equation by the Phase-Amplitude Method (PAM) (Calogero 1967, Babikov, 1967 and 1968). As its name implies, this method yields linked expressions for the amplitude ratios of wave functions and for the phase shifts (and quantum defects). An initial application of this approach dealt with the systematic trend of spin–orbit splitting along the Periodic System (Dehmer, 1973). Various additional applications are presented in this article. An extensive set of calculations of phase shifts, designed from the same point of view but carried out by non-PAM techniques, has been reported by Manson (1969).

The first part of this article describes the historical background and qualitative aspects of our problem, and then discusses the characteristics and limitations of the Hartree–Slater model potentials and those of approaches based on the WKB approximation (Secs. II–V). The second part presents data on the amplitude ratios and on the phase shifts of $s$, $p$, and $d$ wave functions throughout the Periodic System and on the dependence of these parameters on perturbations acting near the nucleus. The data pertain mostly to electrons with energies at the ionization threshold, but include a study of the energy dependence of phase shifts, $d\delta/dE$, and information on how rapidly the effects of shell structure decline as the electron energy increases. A final section reviews the implications of the present knowledge for the various phenomena mentioned in this Introduction.

Although we stress the connection of electron–optical properties of atomic fields with diverse phenomena, we present illustrative data only for neutral atomic systems, more specifically, for an electron moving in the field of a singly charged residual ion. Consequently, the numerical data shown do not apply directly to phenomena, such as electron–atom scattering, which involve an electron moving in the field of a neutral atom. Nevertheless, the point of view is applicable to ionic systems although the detailed systematics would, of course, have to be re-examined. Extension to highly stripped ions is under consideration. Illustrative data pertain to $s$, $p$, and $d$ electrons only, because $f$ electrons do not usually penetrate beyond the outer portions of atoms owing to centrifugal repulsion. Moreover, we confine ourselves to situations where the atomic potential may be adequately regarded as fixed for each kind of atom, in contrast to the important phenomena such as antishielding (Armstrong, 1971), where the effect of interest polarizes or otherwise distorts the rest of the atomic structure substantially.

## II. BACKGROUND

Early attempts to identify a systematic dependence of spectral properties of atoms on their atomic number utilized hydrogenic approximations, even before the advent of quantum mechanics. (See, e.g., Landé 1924.) Even in highly improved treatments one finds it convenient to express results with reference to hydrogenic approximations, as we shall see, because a hydrogenic approximation accounts for the major dependence on atomic number. As a notable example of this approach, consider the formula developed in 1933 by Fermi and Segrè (see also Fermi, 1962, Vol. 1, p. 514) in their study of hyperfine splittings. This formula represents the probability of finding at the nucleus ($r=0$) an optical $s$ electron bound in an orbital state of quantum number $n$, in the form

$$|\Psi(0)|^2 = \frac{Z}{2\pi a^3 I_H}(1-\beta^2 Z^2)^{-1/2}\frac{dE}{dn}. \tag{1}$$

The first factor of this formula, where $a$ is the Bohr radius and $I_H = 13.6$ eV, is the value of $|\Psi(0)|^2$ for a zero-energy, free, nonrelativistic electron in a Coulomb field of atomic number $Z$, normalized per unit energy range. The last factor, denoting the derivative of the energy of a bound electron with respect to its principal quantum number, is drawn from the quantum defect theory, which assumes that a Coulomb field prevails again in the outer fringe of the atom where the optical electron is bound. The middle factor, with the empirical parameter $\beta = 1/139$, is called a relativistic correction. It serves, in fact, to represent the results of extensive numerical calculations, which start from the Dirac equation and use the Thomas–Fermi potential model to propagate the wave function from $r=0$ all the way to the edge of the atom where the field becomes hydrogenic again.

Soon thereafter, Fermi treated the escape of an elec-

tron through the atomic field, in his formulation of the theory of $\beta$-ray emission (Fermi, 1934). In this case he took the value of $|\Psi|^2$ at the nuclear surface simply from the solution of the Dirac equation for the unscreened nuclear field, i.e., as the relativistic form of the first factor on the right of Eq. (1), without commenting on the choice of this approximation. The basis for Fermi's choice was identified explicitly soon thereafter by Rose (1936). Electrons propagate freely—that is without any partial reflection—through a potential field under semiclassical conditions, namely, within the range of validity of the WKB approximation. In other words, transmission through the atomic field focuses or defocuses electrons only to the extent that the WKB approximation fails. The WKB approximation fails within the $K$ shell of any atom, but here the field is approximately Coulombic and its effect can be treated analytically. It fails again for any slow electron near the outer edge of an atom where the field tends once more to be hydrogenic; it fails certainly at the largest radial distance attained by a bound electron. On this basis, our problem reduces to *locating and evaluating* the effect of *simultaneous departures from WKB and from hydrogenic approximations*. Specifically, in the escape of $\beta$ rays, WKB conditions prevail in practice throughout the region outside the $K$ shell. Therefore, the field in this region does not affect the amplitude ratio of the wave function at infinity and near the nucleus, even though it affects its phase. This justifies Fermi's use of the wave function for an *unscreened* field, within the scope of his application.

One may visualize a general formula for representing the electron density at or near a nucleus as having the general structure of the Fermi–Segrè formula, Eq. (1). It would consist of a first factor determined by hydrogenic wave functions of the unscreened nuclear field, embodying the effects of relativity prevailing near the nucleus, as necessary. A second factor would be characteristic of electron transmission through the region occupied by $L, M, \ldots$ shell electrons; this factor would depart from unity only to the extent that a WKB treatment proves inadequate in this range. A third factor, analogous to the last factor of Eq. (1), would depend on the state of the electron in the outer region of the atom. Both the second and third factors are very approximately unity in the case of $\beta$-ray emission, since one deals usually with electrons of nonnegligible energy for which the WKB approximation holds in the outer atom. The remarkable success of approaches related to the Fermi–Segrè formula has attracted attention more recently, forming the subject of studies by Foldy (1958) and by Fröman and Fröman (1972). These studies confirmed that the nonhydrogenic elements of the theory arise from departures from the WKB approximation at intermediate radial distances.

The work leading to the present article was stimulated by several developments: (a) Analysis of photoabsorption by inner-shell electrons showed that photoelectron escape depends strongly on the field in the outer parts of an atom, particularly on potential barriers due to the local dominance of centrifugal forces (see, e.g., Fano and Cooper, 1968). (b) In this and other connections, the net atomic field was found to depend sensitively on the variations of the atomic radius from one element to the next (Rau and Fano, 1968). (c) Application of quantum defect analysis to fine structure data showed a smooth general trend with superposed modulations in their variations along the periodic system (Fano and Martin, 1971). (d) There emerged a widespread increase of activity in calculating still other atomic properties as functions of their positions in the periodic table: scattering phase shifts (Manson, 1969; Griffin *et al.*, 1969); relativity effects (Desclaux and Kim, 1975); spin-orbit coupling (Dehmer, 1973); moments of dipole oscillator strength distributions (Dehmer *et al.*, 1975). Thus, the interest increased in singling out elements common to the various results.

## III. THE MODEL POTENTIAL

Calculation of the electron–optical parameters presupposes the adoption of a model potential. This schematization is inherent to our approach because an electron moving radially through an atom is actually a part of a many-electron system; as a result the potential has nonlocal components and the parameters of interest depend on the state of the complete system. For the purpose of producing broad sets of representative data we have utilized the atomic potentials tabulated by Herman and Skillman (1963), which are derived from the independent-electron HS model. The variations of these potentials along the Periodic System, shown in Fig. 1, follow the variations of atomic radii fairly realistically. Moreover, ample evidence (Fano and Cooper, 1968; Manson, 1969; Dehmer, 1973; Dehmer *et al.*, 1975) exists to show that the HS model is a very useful tool for gaining a realistic first-order approximation to diverse atomic properties. One should, however, bear in mind various limitations of the HS model when assessing the accuracy of the data presented in this article.

Three major approximations are used in the model. First, a local exchange approximation proposed by Slater (1951) permits definition of a local, central potential in the context of the independent-electron model. This exchange potential, expressed as a function of the local charge density, is based on a statistical model of the atom. Therefore, the model does not distinguish between different LS terms of an atomic configuration and hence represents only the average properties of the configuration. This limitation is particularly severe when comparing a HS result with experiments that select only particular terms of a configuration, e.g., the photoabsorption process.

The second approximation of the HS model lies in the use of potentials which are derived from ground-state charge distributions, and therefore are best suited for the calculation of ground state wave functions. Thus we disregard the possible occurrence of vacancies in inner shells and all effects of relaxation of the atomic electrons due to such vacancies or to the very motion of the electron under consideration. The most pronounced effect of this approximation occurs for atoms, such as the alkali metals, whose ground state charge distribution differs significantly from that of the ground ionic state in the region outside the rare gas core. This effect is discussed below in the context of numerical results.

Third, the HS potentials employ a schematic approximation due to Latter (1955). The potential is based on the charge distribution of a neutral atom, and would accordingly vanish outside that charge distribution. In order to treat the motion of an electron in the field of an atomic ion, Latter spliced this neutral potential with that of a unit-charge Coulomb potential at the crossing point of the two potentials, a point indicated in the following as $r = r_0$. This mockup of the effective potential of the ion causes a discontinuity in the derivative of the potential at the joining point, which might produce artifacts in a wave function although none have been explicitly documented to our knowledge. The introduction of the Latter approximation proves very convenient, in a purely operational sense, because it eliminates departures from Coulomb field altogether from the whole range $r \geq r_0$. Thus all numerical calculations can stop at the "cutoff radius" $r_0$, which is of the order of a few Ångstroms. The resulting inaccuracy of the model potential in the region $r \sim r_0$, near the edge of the atom, is troublesome because this region is the seat of the conspicuous effects of shell filling along the Periodic System displayed in Secs. VI–IX. These effects are magnified for $d$ (and $f$) electrons by the near cancellation of the electric and centrifugal potentials and accordingly depend sensitively on the accuracy of the model potential in the range $r \sim r_0$. On the other hand, little profit might ensue from elimination of the Latter approximation in the presence of other inherent inaccuracies of the model potential.

The HS model potential also fails to make allowance for the polarization of the ion by an electron at $r > r_0$. This effect contributes generally a small positive amount, of the order of 0.01, to the phase shifts or quantum defects. It can be readily estimated using the Born approximation form, Eq. (9) below, of the PAM with the perturbation $\Delta U = \alpha e^2/r^4$, at $r \geq r_0$, where $\alpha$ indicates the polarizability of the ion and is of the order of one atomic unit.

The limitations of our model prove serious for the treatment of perturbations that modify appreciably the wave function of several electrons, as in the example of the relativistic correction, which operates near the nucleus only but tends to draw all penetrating orbitals closer to the nucleus (Sec. VIII). This contraction disturbs the self-consistency of the whole potential field and thereby influences the motion of all other electrons (Desclaux and Kim, 1975). No approximation method has been developed to treat this chain of perturbations, short of a full recalculation of the self-consistent field. The same difficulty is met in the treatment of antishielding effects (Armstrong, 1971), as noted in the Introduction.

The model also disregards inelastic interactions, i.e., the possible excitation or ionization of other electrons by the electron of interest in the course of its penetra-

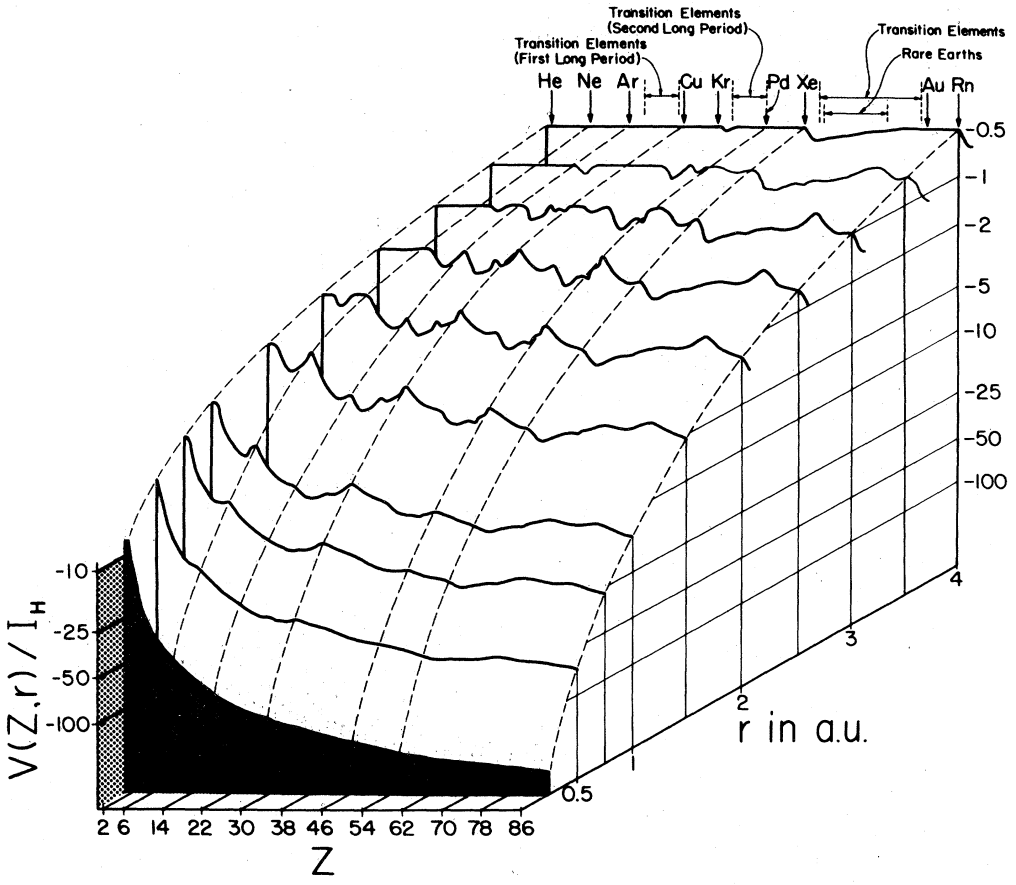


FIG. 1. Relief map of the Herman–Skillman (1963) atomic potentials (from Rau and Fano, 1968).

tion or escape. The probability of inelastic events is generally of the order of only a few percent when the electron energy exceeds the threshold for escape by $\geq$10–50 eV as evidenced by the weakness of the satellites in Auger spectra; at lower escape energies these satellites may reach 20–30% (Krause *et al.*, 1971). Even when they occur, inelastic events need not disturb the penetration or escape severely, but their possible influence should be evaluated for each process.

## IV. THE PHASE-AMPLITUDE METHOD (PAM)

We review here the formulas of the PAM which serve to calculate phase shifts and amplitude ratios directly. Some technical aspects of their application will also be discussed.

Consider the Schrödinger equation

$$\frac{d^2u}{dr^2}+k^2(r)u(r)=0, \quad k^2=\frac{2m}{\hbar^2}[E-V(r)]-\frac{l(l+1)}{r^2}, \tag{2}$$

with alternative atomic potentials $V(r)$ and $U_0(r)$, where

$$V(r)=U_0(r)-U(r), \tag{3}$$

and $U(r)$ may be designed to vanish for large values of $r$, e.g., at $r>r_0$. [The sign of $U$ in Eq. (3) implies that $U$ represents an *increment of attraction* and serves to eliminate negative signs from later equations.] Indicate by $f(r)$ and $g(r)$ a regular and an irregular solution of the equation with potential $U_0$. The objective of PAM is to study properties of the regular solution $u$ of the equation with potential $V$, as explicit functions of $U$, $f$, and $g$. This enables one to incorporate into the so-called "comparison functions," $(f,g)$, the properties of the terms grouped into $U_0$ and to express explicitly the way in which $(f,g)$ are modified by the remaining term $U$ so as to produce the net wave function $u(r)$. (The utility of this technique is illustrated by examples in the following sections.)

One represents $u$ as a superposition of $f$ and $g$ in the form

$$u(r)=\alpha(r)[f(r)\cos\delta(r)-g(r)\sin\delta(r)], \tag{4}$$

with the constraint

$$du/dr=\alpha(r)[(df/dr)\cos\delta(r)-(dg/dr)\sin\delta(r)]. \tag{5}$$

Substitution of Eq. (4) in the Schrödinger equation, followed by analytical manipulation, shows $\delta(r)$ to be given by

$$\delta(r)=W^{-1}(2m/\hbar^2)\int_0^r U(r')[f(r')\cos\delta(r')-g(r')\sin\delta(r')]^2\,dr' \tag{6}$$

or equivalently by

$$\tan\delta(r)=W^{-1}(2m/\hbar^2)\int_0^r U(r')\times[f(r')-g(r')\tan\delta(r')]^2\,dr', \tag{7}$$

while $\alpha(r)$ is given by

$$\ln[\alpha(r)/\alpha(\infty)]=-W^{-1}(2m/\hbar^2)\int_r^\infty U(r')\times[f(r')\cos\delta(r')-g(r')\sin\delta(r')]\times[f(r')\sin\delta(r')+g(r')\cos\delta(r')]\,dr', \tag{8}$$

where $W$ is the Wronskian of $f$ and $g$, often normalized to unity. Equation (6) is a Volterra equation in $\delta(r)$ and can be readily solved numerically; once this is done, Eq. (8) yields $\alpha(r)$ by quadrature. Note that $\alpha(r)$ remains well defined, as the ratio of $u(r)$ to the expression in the brackets of Eq. (4), even in the important limit of $r=0$ where each of these quantities vanishes for $l\neq 0$.

Essential features of the representation (4) of $u(r)$ are the following: (a) $\delta(r)$ represents at each $r$ the phase shift of the wave function $u(r)$ with respect to $f(r)$ induced by the potential $U$ in the interval $0\leq r'\leq r$, provided $g(r)$ is chosen so as to oscillate with a phase 90° behind that of $f(r)$ as $r\to\infty$; (b) $\alpha(r)$ represents a change of normalization induced by $U$. [Hence $U$ modifies the amplitude ratio, which is the main concern of this paper, by the factor $\alpha(r)/\alpha(\infty)$.] (c) different physical questions can be formulated with correspondingly different choices of the initial potential $U_0(r)$ and of the "comparison functions" $f$ and $g$. This flexibility is a convenient feature of the PAM. The basic literature (Calogero, 1967) usually starts from a zero potential, or, more exactly, from the centrifugal potential alone, $U_0(r)=(\hbar^2/2m)\,l(l+1)/r^2$; the corresponding functions $f$ and $g$ are the Riccati-Bessel functions $j_l$ and $n_l$. At the same time it stresses the option of alternative potentials. Thus, Dehmer and Fano (1970) combined the centrifugal potential with the unit-charge Coulomb potential setting $U_0(r)=-e^2/r+(\hbar^2/2m)\,l(l+1)/r^2$ as appropriate to the outer region of an atomic field. The use of Coulomb wave functions requires some attention to their normalization in the regions of $r=0$ and $r=\infty$. This subject has been studied by Seaton (1958) with reference to Quantum Defect Theory; its relevance to PAM has been treated by Dehmer and Fano (1970).

Note the following properties of Eqs. (6) and (8). If $U$ is non-negative (non-positive), $\delta(r)$ is a monotonically increasing (decreasing) function of $r$. Furthermore, if we replace $U$ by $\Delta U$ which is so small that $\delta$ remains $\ll 1$, Eq. (6) reduces to the Born approximation formula

$$\delta(r)\sim W^{-1}(2m/\hbar^2)\int_0^r \Delta U(r')[f(r')]^2\,dr'. \tag{9}$$

On the other hand, the integrand of Eq. (8) contains a factor with alternating sign; hence, $\alpha(r)$ may be amplified or depressed—i.e., the electron may be focused or defocused—depending on the sign of the integrand in different ranges of $r'$. Also, whereas the calculation of the phase shift $\delta(r)$ proceeds outward from the nucleus owing to the boundary condition $\delta(0)=0$, the calculation of the amplitude factor $\alpha(r)$ proceeds inwards starting from unit normalization at $r=\infty$. The analog for $\alpha(r)$ of the Born approximation formula (9) is

$$\alpha(r)\sim\alpha(\infty)\left[1-W^{-1}(2m/\hbar^2)\int_r^\infty \Delta U(r')f(r')g(r')\,dr'\right]. \tag{10}$$

A further form of Eqs. (6) and (8) serves to illustrate their properties. This form is obtained by casting the comparison functions themselves in a phase-amplitude form, that is, by setting

$$f(r)=\gamma(r)\sin\phi(r),\quad g(r)=-\gamma(r)\cos\phi(r), \tag{11}$$

with $\gamma=[f^2+g^2]^{1/2}$ and $\tan\phi=-f/g$. Substitution in (6) and (8) yields

$$\delta(r)=W^{-1}(2m/\hbar^2)\int_0^r U(r')\gamma^2(r')\sin^2[\phi(r')+\delta(r')]\,dr', \tag{12}$$

$$\ln[\alpha(r)/\alpha(\infty)]=W^{-1}(2m/\hbar^2)\int_r^\infty U(r')\gamma^2(r')\times\tfrac{1}{2}\sin 2[\phi(r')+\delta(r')]\,dr'. \tag{13}$$

Equation (12) shows more explicitly than Eq. (6) how the contribution of $U(r')$ to $\delta(r)$ varies, in successive intervals $dr'$, in proportion to the square of the function $\gamma(r')\sin[\phi(r')+\delta(r')]$ which is equal to the exact wave function divided by the amplitude function. Equation (13) shows how the corresponding contribution to $\ln\alpha(r)$ varies, instead, in proportion to the oscillating function $\sin 2[\phi(r')+\delta(r')]$.

As we have seen, the PAM expresses electron–optical parameters directly in terms of integrals over the potential $U(r)$, and thus displays the separate contributions to these integrals by various ranges of $r$. On the other hand, its numerical implementation may not optimize computational efficiency. For example, in Sec. VIII the phase shift of a relativistic wave function will be obtained in terms of a $\Delta U$, representing the difference of relativistic and nonrelativistic Hamiltonians, and of nonrelativistic comparison functions. The calculation of the integrals in Eqs. (6) and (8) is simple in this case, but must be preceded by a separate calculation of the nonrelativistic wave functions. Straightforward solution of both the relativistic and nonrelativistic equations might be faster, while providing sufficient accuracy for the resulting phase shift difference.

Another problem arises when an atomic wave function is expressed in terms of analytically known solutions to the long-range field outside the atom. In the cases we study, the electron moves in a Coulomb field at large $r$ and one is led to choose $(f,g)$ to be solutions of the wave equation for this Coulomb field with unit effective charge. This results in $(f,g)$ functions that do not oscillate within the atom and in large $U$ values at small $r$, for an average size atom. Consequently, the phase and amplitude functions exhibit very sharp variations at small $r$, where they induce nodes in the net wave function by mixing the nonoscillating comparison functions. Such rapid variations are to be expected whenever solutions of a potential are synthesized from solutions of a much weaker field, since the nodes in the solution of the stronger field are generated by admixing over a narrow range the irregular function of the weaker field which is diverging at small $r$. Sample phase functions for zero-energy $p$ waves for $Z=16$, 33, and 51, illustrate this behavior in Fig. 2 showing its general characteristic, namely, a steep step by $\sim\pi$ at the center of each $p$ subshell. It is this step which combines the Coulomb functions with $Z=1$ to generate the inner loops (i.e., halfwaves) of the atomic wave function. These steps may complicate the numerical solution of Eq. (6). One normally generates the functions $(f,g)$ on a coarse mesh, either by solving the Coulomb equation numerically or by generating the functions analytically. Then $\delta(r)$ is generated outward from $r=0$ using a variable mesh and an adequate number of points to extend the solution accurately through the steep steps in Fig. 2. Although we have not performed timing tests, the forthright solution of the Schrödinger equation with the potential $V=U_0-U$ is clearly more efficient than employing the PAM equations, if one is interested only in calculating the net phase shift.

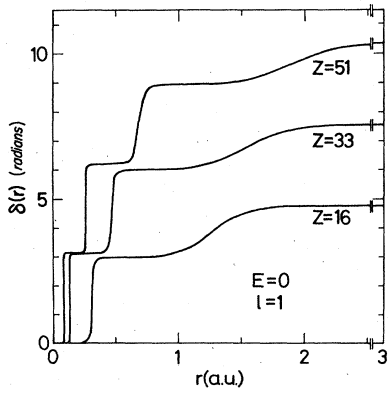


FIG. 2. Phase functions obtained by using Coulomb waves with $Z=1$ as comparison functions.

The data on the amplitudes and phase shifts shown in the following sections illustrate the dispersion relation which presumably holds between $\ln\alpha(0)$ and $\delta(r=\infty)$ and which causes each of these quantities to peak wherever the other increases fastest as a function of energy.[1] We say "presumably" because the applicability of this relation to the specific circumstances of our treatment does not appear to have been investigated explicitly. The matter hinges on the analyticity of the expression, derived from Eqs. (6) and (8),

$$\ln\Phi=\ln[\alpha(0)/\alpha(\infty)]+i\delta(\infty)$$
$$=W^{-1}(2m/\hbar^2)\int_0^\infty U(r')\,[f(r')\cos\delta(r')-g(r')\sin\delta(r')]\times[g(r')+if(r')]\exp[-i\delta(r')]\,dr'. \tag{14}$$

[1] The outgoing and the ingoing portions of a standing wave function with unit amplitude at $r=0$ can be expressed at large $r$ as an $r$-dependent factor times a coefficient of the form $[\alpha(\infty)/\alpha(0)]\exp\pm i\delta_\infty$. Accordingly, the amplitude and the phase shift constitute the modulus and phase of a complex number. On the other hand, dispersion relations—analogous to the Kramers–Kronig relations (Landau and Lifshitz, 1960)—hold between the real and the imaginary parts of a complex analytic function of energy, rather than between its modulus and phase. To convert the modulus and phase of a function into the real and imaginary parts of another function, one simply replaces the initial function by its logarithm; in our case, the real part of the new function is $\ln[\alpha(\infty)/\alpha(0)]$ and its imaginary part is $\pm\delta_\infty$. A dispersion relation will link $\ln[\alpha(\infty)/\alpha(0)]$ and $\delta_\infty$ if the function (14) has the appropriate analytic properties. The amplitude function $\alpha(\infty)$ is set to unity in Eq. (14).

The function $\Phi$ is the analog, for our problem, of the Jost function of scattering theory. The usual Jost function (see, e.g., Newton 1960) is an analytic function of $k_\infty = (2mE/\hbar^2)^{1/2}$ provided the full potential $V(r)$, $0 \leq r \leq \infty$, meets certain conditions that exclude a long range Coulomb behavior. In our problem, this behavior is taken into account by the use of PAM with Coulomb comparison functions, whereby the residual potential $U(r)$, confined to $r \leq r_0$, meets the required conditions. For such a truncated potential Calogero formulates a dispersion relation (Calogero, 1967, p. 36) equivalent to

$$\ln[\alpha(0,k_\infty)/\alpha(\infty,k_\infty)] = -\pi^{-1}P\int_{-\infty}^{\infty} dp\,(p-k_\infty)^{-1}\delta(\infty,p) + \sum_{j=1}^{n}\ln[1+q_j^2/k_\infty^2], \tag{15}$$

where $\{-\hbar^2 q_j^2/2m\}$ represents the energies of the finite set of bound states of the potential $U$, and where $P$ specifies principal part integration at $p \sim k_\infty$. The derivation is in the context of free-particle comparison functions; Calogero (1967) also states that PAM results hold broadly irrespective of the nature of comparison functions, but makes no further explicit reference to the dispersion relation. In practice, $\alpha(0,k_\infty)$ and $\delta(\infty,k_\infty)$ are seldom known over the full range of the energy parameter $k_\infty$; Eq. (15) and analogous relations serve then mostly to illustrate the quasisingular behavior of $\alpha$ (or $\delta$) which results when the main contribution to the integral in Eq. (15) stems from a narrow range of integration, $p \sim k_\infty$.

## V. THE WKB APPROXIMATION FOR ATOMIC FIELDS

In approaching our problem it seemed desirable to see how one could compute directly the effect of departures from the WKB approximation. To the extent that this approximation holds over most of the atomic field outside the $K$ shell, one should be able to demonstrate directly that the solution of the Schrödinger equation over this range contributes to a Fermi–Segrè-type formula, Eq. (1), a factor close to unity. A formalism suited to this purpose is available in the PAM literature, particularly on p. 43 and p. 187 of Babikov (1968). We summarize it as follows.

The solution of the radial Schrödinger equation (2) can be expressed in terms of an amplitude function $A(r)$ and a phase function $\Delta(r)$ defined implicitly by the pair of equations

$$u(r) = A(r)k(r)^{-1/2}\sin[\phi(r)+\Delta(r)], \tag{16a}$$

$$du(r)/dr = A(r)k(r)^{1/2}\cos[\phi(r)+\Delta(r)]; \tag{16b}$$

the usual WKB phase function

$$\phi(r) = \int^r k(r')\,dr' \tag{16c}$$

serves here as a comparison phase. This formulation pertains to the classically accessible region where $k$ is real; the lower limit of integration in Eq. (16c) relates to the definition of $\Delta$. Equations (16a) and (16b) transform the Schrödinger equation (2) into the pair of first-order nonlinear equations,

$$\frac{d\ln A}{dr} = \frac{1}{2}\frac{d\ln k}{dr}\cos[2(\phi+\Delta)], \tag{17a}$$

$$\frac{d\Delta}{dr} = -\frac{1}{2}\frac{d\ln k}{dr}\sin[2(\phi+\Delta)]. \tag{17b}$$

According to these equations, both the amplitude $A$ and the phase $\Delta$ vary with $r$ only to the extent that $k$, i.e., the reciprocal of the wavelength $\lambda\!\!\!^{-}$, varies. Specifically, the WKB approximation holds insofar as the numerical parameter

$$\epsilon = \frac{d\lambda\!\!\!^{-}}{dr} = \frac{d}{dr}\left(\frac{1}{k}\right) = \frac{1}{k}\frac{d\ln k}{dr} = -\frac{d\ln k}{d\phi} \tag{18}$$

is much smaller than unity. The Eqs. (17) can be expressed in terms of $\epsilon$ by taking $\phi$ as an independent variable, yielding

$$\frac{d\ln A}{d\phi} = -\frac{\epsilon}{2}\cos[2(\phi+\Delta)], \tag{19a}$$

$$\frac{d\Delta}{d\phi} = \frac{\epsilon}{2}\sin[2(\phi+\Delta)]. \tag{19b}$$

To evaluate the parameter $\epsilon$, it is convenient to express the potential in terms of an effective atomic number by writing $V(r) = -Z_{\rm eff}(r)\,e^2/r$. Equation (2) gives then

$$k^2 = \frac{2m}{\hbar^2}\left[E + \frac{Z_{\rm eff}(r)e^2}{r}\right] - \frac{l(l+1)}{r^2} = \frac{2mE}{\hbar^2} + \frac{2Z_{\rm eff}(r)}{ar} - \frac{l(l+1)}{r^2}, \tag{20}$$

where $a$ is the Bohr radius, and

$$\epsilon = \frac{d(k^{-1})}{dr} = \frac{(Z_{\rm eff}/ar^2)(1 - d\ln Z_{\rm eff}/d\ln r) - l(l+1)/r^3}{[k_\infty^2 + 2Z_{\rm eff}/ar - l(l+1)/r^2]^{3/2}} = \frac{1}{(\rho_{\rm eff})^{1/2}}\frac{1 - d\ln Z_{\rm eff}/d\ln r - l(l+1)/\rho_{\rm eff}}{[2 + k_\infty^2 r^2/\rho_{\rm eff} - l(l+1)/\rho_{\rm eff}]^{3/2}} \tag{21}$$

where $k_\infty = (2mE/\hbar^2)^{1/2}$, as above, and $\rho_{\rm eff} = Z_{\rm eff}(r)r/a$ represents $r$ in units of a "local value" of the Bohr radius, $a/Z_{\rm eff}(r)$. In the asymptotic region, outside the charge distribution of the ion core, $Z_{\rm eff}$ becomes unity yielding,

$$\epsilon = \frac{1}{\rho^{1/2}}\frac{1 - l(l+1)/\rho}{[2 - l(l+1)/\rho]^{3/2}}, \quad \rho = r/a, \quad \text{for } k_\infty = 0,\ r > r_0. \tag{22}$$

Figure 3 shows sample plots of the parameter $\epsilon$ for $s$ and $p$ electrons with zero energy at $r = \infty$. In the interior of the atom, breakdown of the WKB approximation is represented by large values of $\epsilon$ near $r = 0$ for $s$ electrons and near the classical "turning point" due to the centrifugal potential barrier for $p$ and higher-$l$ electrons. For $d$—and even more strikingly for $f$—electrons a second region of breakdown occurs for $k_\infty \sim 0$ in the outer region of the atom where the centrifugal repulsion again tends to dominate over the electrostatic attraction and thus to generate a second classically forbidden region. Our example of zero kinetic energy emphasizes the non-WKB circumstances in the atom, and is pertinent to the data in the following sections. However, we emphasize again that these high-$l$ effects on

the edge of the atom are suppressed and the $\epsilon$ values at intermediate values of $r$ are generally reduced as the electron energy increases.

Figure 4 shows sample values of the quantity $Q = |d\ln Z_{\rm eff}/d\ln r|$ which plays a central role in the behavior of $\epsilon$ described by Eq. (21). Irregularities of $Q$ reflect the shell structure of the charge distribution or, equivalently, of $dZ_{\rm eff}/dr$; these oscillations appear more pronounced in the outer shells because they are suppressed at small distances where the denominator of the quantity $d\ln Z_{\rm eff}/d\ln r = (dZ_{\rm eff}/dr)/(Z_{\rm eff}/r)$ is large. As expected, these features vary along the Periodic System, depending on the electronic configuration of the ion. On the whole, $Q$ changes considerably in the region 0 to 2.5 a.u., reaching a maximum of about 1.2 to 1.4.

Figure 3 demonstrates clearly that $\epsilon$ is, in fact, never very small for energies near threshold; its peak in the middle of the range corresponds to the peak of $Q$, and shows the shell structure features due to $Q$. We conclude from the figures that better-than-WKB treatments are required at such energies. Indeed the Fermi–Segrè and analogous calculations of the 30's did involve numerical integration of the radial wave equations. On the other hand, the values of $\epsilon$ decrease as the electron energy rises above threshold, through the influence of the $k_\infty^2 r^2$ term in the denominator of Eq. (21). Numerical estimation of the value of $\epsilon$ given by Eq. (21) is facilitated by use of the approximate formulas $d\ln Z_{\rm eff}/d\ln r = -Q \sim -1$ and $\rho_{\rm eff} \sim 0.4Z^{2/3}$ in the important range $0.25 \leq r \leq 2$ a.u.[2]

Whenever the energy of an escaping electron is sufficiently high to make $\epsilon$ negligible, WKB conditions hold in the intermediate and outer shells; consequently the hydrogenic formulas applicable near the nucleus become adequate, in accordance with Sec. II. This should be the case, e.g., throughout the energy range at which the standard formulas of $\beta$-decay theory have been applied. The same circumstances obtain for most of the usual applications of hydrogenic formulas to bremsstrahlung, Auger effect, etc. We have in mind here primarily the processes occurring within the $K$ shell; however, these considerations can be applied to intermediate shell processes with the proviso that hydrogenic formulas be suitably adjusted, e.g., with screening corrections. However, caution must be exercised when extending applications to the escape of electrons with energy not much in excess of threshold; examples of near-threshold effects are given in the following sections.

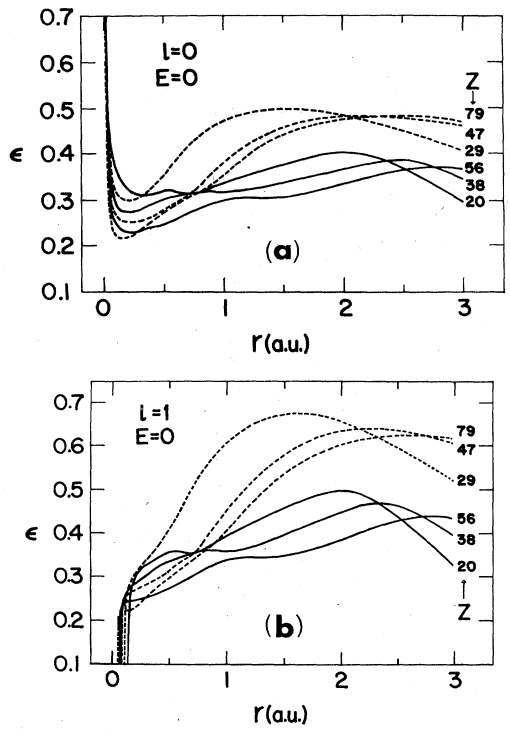


FIG. 3. Values of the WKB parameter $\epsilon = d\chi/dr$ at $E=0$ for various elements; (a) $l=0$, (b) $l=1$.

## VI. $Z$-DEPENDENCE OF THE AMPLITUDE RATIO $\alpha_l(0)/\alpha_l(\infty)$

The first electron–optical parameter which we consider is the $Z$ dependence of the amplitude ratio for zero-energy waves. Its values for $0 \leq l \leq 2$ are presented in Fig. 5 in terms of a function $\Sigma(l,Z)$ defined below. For this application, we adopt as comparison functions the eigenfunctions of a Coulomb field with charge $ze$ which, for $E=0$, have the large $r$ forms (Bethe and Salpeter, 1957)

$$f \to (ar/2z)^{1/4}\sin\omega, \tag{23a}$$

$$g \to -(ar/2z)^{1/4}\cos\omega, \tag{23b}$$

where

$$\omega = (8rz/a)^{1/2} - (l+\tfrac{1}{4})\pi .$$

This choice of $(f,g)$ reduces $\alpha(\infty)$ to unity; indeed, $\alpha(r)$ remains constant at unity outside the charge distribution of the parent ion, which in the HS model, vanishes for

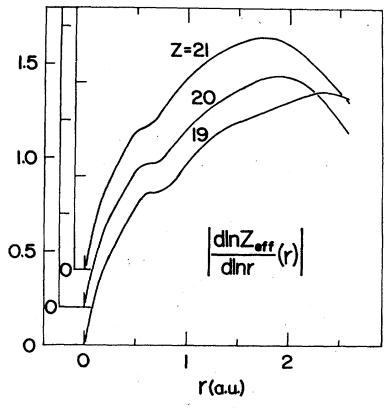


FIG. 4. Values of the atomic field function $Q = |d\ln Z_{\rm eff}(r)/d\ln r|$ for sample elements at $E=0$.

[2]The existence of this convenient approximate formula for $\rho_{\rm eff}$, implying that $Z_{\rm eff}(r) \sim 0.4Z^{2/3}a/r$ over a broad range, is not widely known but is verified easily by inspection of Tables of the Herman–Skillman (1963) or Thomas–Fermi (Gombás, 1949) potentials.

all $r > r_0$. In the following we set $z = 1$.

With $\alpha(\infty, Z)$ thus set to unity, we represent the amplitude ratio in the form

$$[\alpha_l(0,Z)/\alpha_l(\infty,Z)]^2 = \alpha_l^2(0,Z) = Z^{2l+1}\Sigma(l,Z). \quad (24)$$

This expression is analogous to the Fermi–Segrè formula (Eq. 1) in that the first factor on its right-hand side represents the dominant contribution to the $Z$ dependence due to the Coulomb field near $r = 0$, while the factor $\Sigma(l,Z)$, plotted in Fig. 5, represents the non-WKB effect of the remainder of the atomic field. We neglect relativistic effects in this treatment. Consequently, the deviations of $\Sigma(l,Z)$ from unity indicate how much the propagation of a zero-energy electron through the atomic shells departs from the WKB approximation.

Inspection of Fig. 5 shows sharp departures from unity which follow the structure of the Periodic System, superimposed on a smoother average trend. For $l = 0$ this average trend is flat and near unity. For $l = 1$ and even more so for $l = 2$, the average $\Sigma(l,Z)$ is depressed significantly for low $Z$ and then gradually returns toward unity as $Z$ increases. This average behavior is caused by the centrifugal potential which inhibits the deep penetration of non-$s$ electrons into the atomic core, and thus prevents the amplitude ratio from rising as fast as implied by the factor $Z^{2l+1}$ in Eq. (24).[3] The relative importance of this "centrifugal" screening diminishes as $Z$ increases, so that the average value of $\Sigma(l,Z)$ tends toward the hydrogenic value $\Sigma(l,Z) = 1$. Note that for $l = 2$, $\Sigma(l,Z)$ remains small for all $Z < 20$ as no orbit penetrates inside the centrifugal barrier on the edge of the atom at zero energy. As pointed out in Sec. II, $\Sigma(l,Z)$ should approach unity as the electron kinetic energy increases, so that for higher values of $E$, the curves in Fig. 5 should approach unity uniformly.

Now we focus on the periodic structure of $\Sigma(l,Z)$ and on its relation to the filling of the subshells in the Periodic Table. An important consideration here is evident from the expression of $\ln[\alpha(r)/\alpha(\infty)]$ in Eq. (13) in terms of the oscillating function $\sin 2[\phi + \delta]$. Since $\gamma^2 U$ is nonnegative in our problem, even quadrants of $\phi + \delta$ contribute negatively to the integral in Eq. (13), while odd quadrants contribute positively. A combination of this representation of $\alpha_l(0)$ with knowledge of the nodal structure of atomic radial wave functions permits an analysis of the sharp structures in Fig. 5. We can further note that in the closed-shell region of the atom the potential well is deep and the inner loops of the wave function vary smoothly with $Z$. Each loop over which $\phi + \delta$ increases by $\pi$, contributes one positive and one negative part to the integral in Eq. (13). These contributions cancel somewhat and produce a net smooth increase without any periodic structure in $\Sigma(l,Z)$. Hence, the periodic variations of $\Sigma(l,Z)$ stem from the valence region of the potential. It is in this region of space, outside the closed shells but within the region of finite electron density, that the atomic shell structure manifests itself. Moreover, $\gamma^2(r)$ will be relatively smooth in this critical region so that consideration of the factor $\sin 2[\phi + \delta]$ is sufficient for our purposes.

As a specific example, we analyze the variation of $\Sigma(l,Z)$ over the elements Xe ($Z = 54$) through Rn ($Z = 86$). Within this range, subshells with $l = 0, 1, 2, 3$, are filling. The first of these elements is xenon, whose $5p$ subshell has just filled and has a wave function with exactly four loops overlapping the compact (closed-shell) rare gas potential $U$. This atom corresponds to a local minimum in the function $\Sigma(1,Z)$, associated with an even number of quadrants of the wave function in the interval $[0, r_0]$. Likewise, all rare gases represent local minima of $\Sigma(0,Z)$. For Xe, this occurs because five complete $l = 0$ loops lie in the range $[0, r_0]$. On the other hand, Xe is nearer a local maximum for $l = 2$, because incipient contraction of the $5d$ subshell causes the leading quadrant of the third $l = 2$ loop to overlap with $U$, resulting in an uncanceled positive contribution to the integral in Eq. (13).

Going from Xe to Cs, we note a dramatic change. The $6s$ subshell becomes occupied causing a sudden expansion of the radius $r_0$ from 3.57 to $4.15a$. For $l = 0$, the enhanced overlap between the more extended $U$ and the eleventh quadrant of the $6s$ wave function causes a very sharp rise of $\Sigma(0,Z)$. This particular effect may, however, be overemphasized by the inaccuracy implicit in utilizing the HS field of a neutral atom to study the mo-

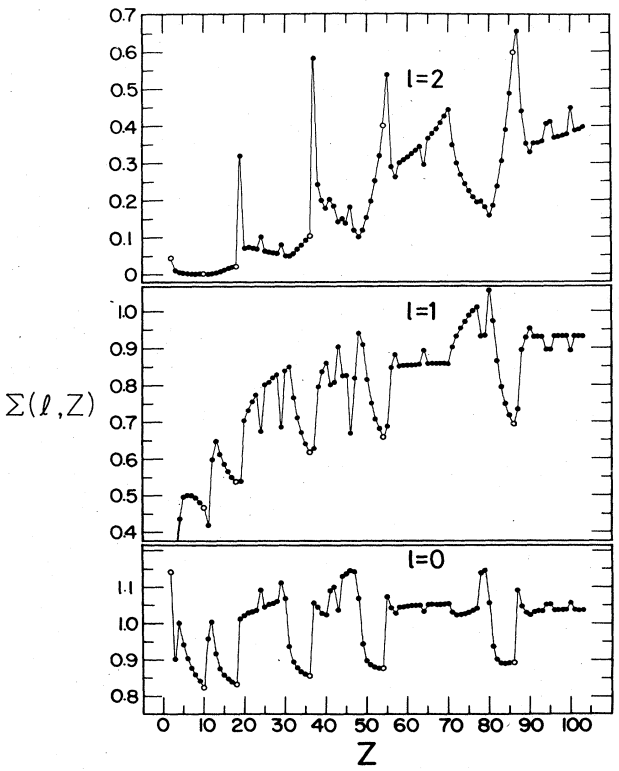


FIG. 5. Reduced values of the amplitude ratio $\alpha(r=0)/\alpha(r=\infty)$ in the form of $\Sigma(l,Z) = [\alpha^2(r=0)/\alpha^2(r=\infty)]/Z^{2l+1}$.

[3] This effect of inner screening is often represented (Casimir, 1962) by replacing $Z^{2l+1}$ by $[(Z - \sigma(Z)]^{2l+1}$ in Eq. (24) where the screening number $\sigma(Z)$ replaces the factor $\Sigma(l,Z)$. The value of $\sigma(Z)$ implied by spin–orbit coupling data for $p$ electrons has been found to vary from 2 for $Z = 5$ to 9 for $Z = 90$ (Fano and Martin, 1971). This empirical method of accounting for nonhydrogenic behavior has unphysical implications which have been pointed out elsewhere (Fano and Martin, 1971, and Dehmer, 1973).

tion of a valence electron in the field of the residual ion. That is, whereas a $Cs^+$ ion with an open-shell configuration, e.g., $4d^9 5p^6 6s$, is indeed much larger than $Xe^+$; the $Cs^+$ ground state $4d^{10}5p^6$ is much smaller. Therefore, when applying Fig. 5 to ground-state ion cores only, one should rather expect a shift in this sudden rise towards the next higher $Z$ value. Analogous qualifications pertain to the other alkali metals, and, to a lesser extent, to other neutral atoms containing one electron outside a closed-shell core. For Ba a slight decrease of $\Sigma(0,Z)$ is observed in Fig. 5 as the $6s$ subshell closes. For $p$ waves, $\Sigma(1,Z)$ also rises as an $s$ subshell fills for reasons similar to the case of $s$ waves. However, the jump is less abrupt here and it lags behind that of the $s$ wave, reflecting the delay between the penetration into the core of the valence loop of the $p$ wave relative to that of the $s$ wave. For $l=2$, a peak in $\Sigma(2,Z)$ at Cs is followed by a plummeting at Ba caused by a sudden contraction of the $5d$ subshell inside the centrifugal barrier; this effect occurs systematically one atomic number before a high-$l$ subshell becomes occupied in the ground state (see, e.g., Griffin *et al.*, 1969).

The large peak in $\Sigma(2,Z)$ occurring in the vicinity of the alkali metals is related to the familiar shape resonance which is observed in many phenomena, e.g., elastic and inelastic electron scattering (Schulz, 1973) and photoabsorption (Fano and Cooper, 1968). A shape resonance is a phenomenon associated with the motion of a single particle with energy close to the edge of a deep potential well (Blatt and Weisskopf, 1952). It occurs for an electron–ion or electron–atom potential field mainly when it exhibits a centrifugal barrier because otherwise the edge of an atomic field would be too diffuse. As discussed extensively elsewhere (see, e.g., Fano and Cooper, 1968 and references therein) many situations exist wherein the potential well inside the barrier can support a narrow band of quasibound states at some energy near or below the top of the barrier. This circumstance causes the amplitude ratio $\alpha_l(0)/\alpha_l(\infty)$ to peak over this band of total energies. The conventional way of observing this resonance phenomenon is to "tune" the total energy so that the net well inside barrier is sufficiently attractive to support a quasibound state. An alternative way is to tune the strength of the inner well by altering the nuclear charge, as displayed in Fig. 5. The sharp peaks in $\Sigma(2,Z)$, therefore, correspond to eigen-atomic numbers at which the inner well supports a quasibound $d$ state at zero energy.

Between $Z=57$ and $Z=71$, the $4f$ subshell is filling. The $l=0,1$ curves in Fig. 5 are very flat in this range, except for minor fluctuations at the particular elements with $Z=57$, 64, and 71, which differ from the others by having one electron shifted to a $5d$ orbit, a physical effect (Cotton and Wilkinson, 1967) reflected in the HS model. This flat behavior is to be expected since the $4f$ shell has a radius ($r\sim 1$ a.u.) smaller than the $6s$ and $6p$ valence subshells. These subshells are thus shielded from the progressive increase in nuclear charge by the progressive addition of $4f$ electrons localized deeper within the atom. Only the $l=2$ curve varies in this range of $Z$; its rise accompanies the shrinking of the inner $4d$ subshell which is only partially screened from the increase in nuclear charge.

At $Z=72$, the $5d$ subshell starts filling up extensively, causing the value of $\Sigma(2,Z)$ to decrease suddenly as the $5d$ wave function attains full overlap with $\Delta U$ with resulting cancellation between its positive and negative contributions to the integral of Eq. (13). Along this sequence, the $6p$ loop begins to move into the interval $[0,r_0]$ prior to its occupation at $Z=81$. This causes the fifth quadrant of the $6p$ wave function to yield an increasingly positive contribution to the integral in Eq. (13). On the other hand, the $l=0$ curve is rather flat between $Z=72$ and 77, because the $6s$ subshell is already full and the onset of $7s$ filling is not yet imminent. At $Z=78$, 79, both $\Sigma(0,Z)$ and $\Sigma(1,Z)$ jump by ~10% as the HS model field reflects the transfer of a $6s$ electron to the $5d$ subshell, a well-known discontinuity (Cotton and Wilkinson, 1967).

From $Z=81$ to 86, the $6p$ subshell fills, completing the cycle at radon. Along this sequence, $\Sigma(1,Z)$ steadily decreases reflecting the growing overlap between the even quadrant of the outer loop of the $6p$ wave function and $U$. On the other hand, $\Sigma(0,Z)$ decreases only slightly in this range, while $\Sigma(2,Z)$ rises owing to an increase in penetration of the leading quadrant of the $6d$ loop in preparation for its sudden contraction at $Z=88$.

The characteristic $Z$ dependence of $\alpha_l(0)/\alpha_l(\infty)$ embodied in Fig. 5 should manifest itself in the $Z$ dependence of any atomic parameter which depends on the behavior of radial wave functions at small $r$. We discuss two main examples here—spin–orbit coupling and hyperfine interaction, and indicate several other examples. In these examples we cast the $Z$ dependence of each parameter as a product of two factors so that the major $Z$ dependence is contained in one factor which depends solely on $\alpha_l(0)/\alpha_l(\infty)$ whereas the other factor is nearly $Z$ independent.

### A. Spin-orbit coupling

In a previous study, Dehmer (1973) applied this approach to the $Z$ dependence of spin–orbit coupling for zero-energy $p$ waves. In that study, the spin–orbit coupling strength was represented by $\Delta\mu$, the difference in quantum defect between the fine structure states. This parameter may be described as the spin–orbit energy of states normalized per unit energy range; accordingly, it is dimensionless, varies smoothly through the ionization limit, and characterizes the strength of spin–orbit coupling at $E=0$ conveniently. The value of $\Delta\mu$ is given by the perturbation theory expression

$$\Delta\mu = \frac{1}{2}\left(\frac{\hbar}{mc}\right)^2 \int_0^\infty \frac{1}{r}\left(\frac{dV}{dr}\right) P_\epsilon^2(r)\,dr\,, \tag{25}$$

where $P_\epsilon$ is a zero-energy spin independent $p$ wave evaluated for the atomic field $V$ and normalized per unit energy range. Equation (25) assumes $\Delta\mu \ll \mu$ and is analogous to the Born approximation form given in Eq. (9), with $W=1$, $\Delta U = r^{-1}(dV/dr)$,[4] and $f=P_\epsilon$. For high

[4]Note that

$$\frac{1}{r}\frac{dV}{dr} = \frac{Z_{\rm eff}}{r^3}\left(1 - \frac{d\ln Z_{\rm eff}}{d\ln r}\right) = \frac{Z_{\rm eff}}{r^3}(1+Q)\,,$$

where $Q$, the parameter defined in Sec. V, is $\ll 1$ through most of the range contributing to the integral in Eq. (25).

principal quantum numbers $n$, $\Delta\mu$ is related to the spectroscopic strength parameter $\zeta_{nl}$ by

$$\Delta\mu \sim \zeta_{nl} n^{*3}/2I_H = \zeta_{nl}(n-\mu)^3/2I_H . \quad (26)$$

Inspection of the profile of the integrand of Eq. (25) (Fig. 6) shows that it peaks remarkably close to $r \sim a/Z$, i.e., at the center of the $K$ shell. Moreover, the value of the integrand at its maximum was found to be proportional to $\alpha_1^2(0,Z)$. These remarks suggested replotting the ratio of the integrand to $\alpha_1^2(0,Z)$ as a function of $Zr$. The result, shown in Fig. 7, reveals that the integrand thus renormalized is an approximately universal function. Actually, the areas of the two curves in Fig. 7 differ by ~7%,[5] with most of the difference accumulating beyond the $K$ shell. Universality of the plot in Fig. 7 would imply the scaling formula

$$\Delta\mu = C\,\alpha_1^2(0,Z)/Z = CZ^2\Sigma(1,Z), \quad (27)$$

where $C$ is the area under the quasiuniversal curve, with typical values

| H | Ar | Kr | Xe | |
|---|---|---|---|---|
| $C$ = 1.20 | 1.13 | 1.05 | 1.01 | $\times 10^{-5}$. |

Using the values of $\Sigma$ in Fig. 5, together with a multiplicative correction for the relativistic effect (Casimir, 1962) and an approximate value of $C = 1.0\times10^{-5}$, one obtains

$$\Delta\mu = 2.45\times10^{-6}Z^{2.33} . \quad (28)$$

The power of $Z$ in Eq. (28) agrees very well with the power law observed in the experimental data compiled by Fano and Martin (1972) and represented by

$$\Delta\mu = 2.05\times10^{-6}Z^{2.33} . \quad (29)$$

Note that this observed power law deviates significantly from the Coulombic $Z^2$ power law which would obtain in the WKB approximation.

The ~20% difference between the coefficients in Eqs. (28) and (29) has not yet been satisfactorily explained. On the one hand, the theoretical calculation is based on an approximate atomic field, with a relativistic correction factor only, and hence it is not expected to be highly accurate. On the other hand, the experimental data are sparse and could lead to an extrapolation error in the curve fitting. Moreover, not all data have been extrapolated to the series limit; an adjustment of the order of the difference of the two coefficients might result from improved analysis. This question can only be resolved in the light of more extensive experimental data extrapolated to the series limit.

Taking a broad view of this analysis, we see that the dominant $Z$ dependence can, in fact, be simply cast in terms of the ratio of $\alpha_l(0,Z)/\alpha_l(\infty,Z)$ whose variations we have analyzed. Unfortunately, the data collected by Fano and Martin (1971) are too sparse to exhibit the detailed fine structure predicted by Fig. 5. Our confidence that this structure is at least qualitatively correct rests on the success experienced in using the HS model to predict realistically the dependence of other atomic parameters on the atomic number (Fano and Cooper, 1968, Sec. 4; Inokuti *et al.*, 1975; Dehmer *et al.*, 1975). In order to achieve a more satisfactory comparison between experiment and theory, it is necessary that the practice be adopted of presenting experimental spin–orbit data in the form of a quantum defect difference, $\Delta\mu_l$, rather than of the strength parameter $\zeta_{nl}$ itself. This suggestion is not designed to make the theorist's job easier but rather is prompted by extensive experience (Fano, 1975a) in applying quantum defect theory to an assortment of problems in atomic physics. This experience indicates that transformation of data on level positions and shifts to the quantum-defect scale removes their main energy dependence and thus makes parameters for different levels more directly comparable. Consequently, data reported in this way are characteristic of entire excitation channels, below and above their respective ionization thresholds, thus permitting direct comparison with our zero-energy mapping.

The $Z$ dependence of the spin–orbit interaction for

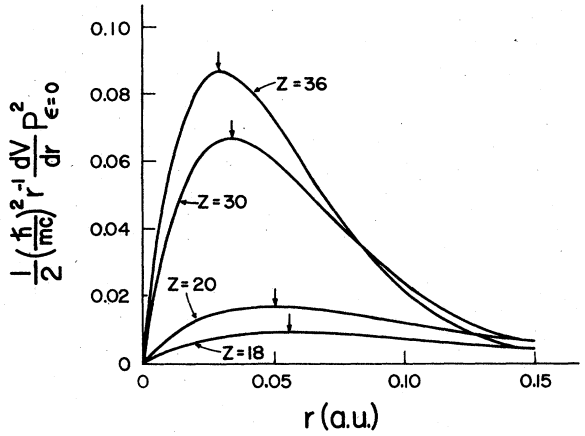


FIG. 6. Integrand of Eq. (25) for zero-energy $p$ waves with $Z = 18, 20, 30, 36$. The arrows correspond to the radial distances $r = a/Z$.

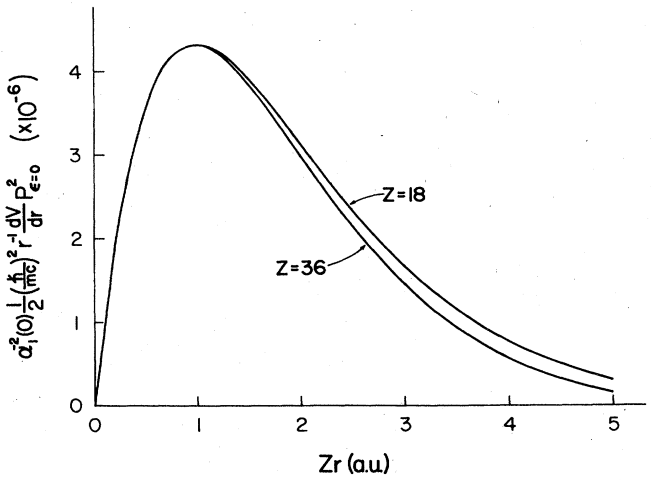


FIG. 7. Integrand of Eq. (25) for Ar and Kr, divided by $\alpha^2(0,Z)$, and plotted as a function of $Zr$.

[5]Figure 7 is a revised version of Fig. 3 of the earlier work (Dehmer, 1973) in which the difference appeared to be smaller, approximately 1% to 2%.

$l=2$ and 3 may be analyzed proceeding along the following lines. To begin with, one should extend to higher $l$ the characterization of the radial location of the integrand in Eq. (25). Since the spin–orbit interaction is confined to the small $r$ region, which is dominated by the Coulomb field of the nucleus, we utilize here hydrogenic formulas. In this approximation the mean radius of the integrand in Eq. (25) can be described as the average of $r$ weighted by the electron density multiplied by $r^{-3}$ and is accordingly represented by $\langle r^{-2}\rangle/\langle r^{-3}\rangle$. This mean radius is energy independent,[6] peaks one shell nearer the nucleus than the shell containing the first radial antinode of angular momentum $l$, and is skewed to large $r$. Therefore, the spin–orbit interaction is localized well within the radius of the first antinode of the radial wave function of a given $l$, and its profile resembles the one shown in Fig. 7. Consequently, the screening of the spin–orbit interaction will saturate near the atomic number at which the first subshell of a given $l$ becomes fully occupied, that is, $Z=30$ for $l=2$ and $Z=71$ for $l=3$. As a result, the profile of the integrand in Eq. (25) becomes approximately $Z$-independent when plotted as a function of $Z_{\rm eff}r$ and divided by the square of the amplitude function at $r_{\max}$. This suggests a general form for $\Delta\mu_l$ which is analogous to Eq. (27) but applies to all $l<4$,

$$\Delta\mu_l(Z)\cong C_l\frac{[\alpha_l(r_{\max})/\alpha_l(\infty)]^2}{Z_{\mathrm{eff},l}}H_l$$

$$=C_l Z^{2l+1}\Sigma(l,Z)\frac{[\alpha_l(r_{\max})/\alpha_l(0)]^2}{Z_{\mathrm{eff},l}}H_l\,, \qquad (30)$$

where $\alpha_l(r_{\max})$ is the amplitude function at the peak of the spin–orbit integrand (the mean $r$ value of the integrand would also suffice for our purposes), $C_l$ is the area under the "universal" integrand, $Z_{\mathrm{eff},l}$ is the effective charge at $r_{\max}$, and $H_l$ is Casimir's (1962) relativistic correction. The extreme right-hand side of Eq. (30) expresses the result in terms of the factor $\Sigma(l,Z)$ plotted in Fig. 5, and of the residual factors $[\alpha_l(r_{\max})/\alpha_l(0)]^2$ and $H_l$. For $l=1$, the first of these factors is very nearly unity while the relativistic correction $H_l$ is significant, ranging up to ~1.25. For higher $l$, $H_l$ will be negligible, but the factor $[\alpha_l(r_{\max})/\alpha_l(0)]^2$ may have a more significant, though smooth, effect on $\Delta\mu_l(Z)$ caused by changes in screening experienced in the region of $r_{\max}$. Variations of the scaled integral $C_l$ can also be expected to exhibit smooth but nonnegligible variations with atomic number, probably amounting to ~10 to 20% for the ranges indicated above. Estimations of the slowly varying factors which depend on the field at small $r$, namely, $[\alpha_l(r_{\max})/\alpha_l(0)]^2$ and $C_l$, may be obtained conveniently using an analytic procedure for producing small-$r$ radial wave function by McEnnan and Pratt (1975). These factors are nonnegligible and must be evaluated numerically for more quantitative treatments. In addition, since $\Delta\mu_l$ is very small for $l>1$, the effect of perturbations neglected in our treatment may become so important as to obscure the $Z$ dependence predicted by Eq. (30). Nevertheless, this representation provides a useful frame of reference in which the central role of the parameter $\alpha_l(0)$ is exhibited explicitly.

### B. Hyperfine interaction and other inner-shell phenomena

In the most important and yet elementary case, $J=S=\frac{1}{2}$, the hyperfine interaction leads to the appearance of a doublet, $F=I\pm\frac{1}{2}$, with a splitting given by

$$E_{I+1/2}-E_{I-1/2}=(8\pi/3I)\,\mu_N\mu_e(2I+1)\Psi_n^2(0)\,, \qquad (31)$$

where $I$ is the nuclear spin quantum number, $\mu_N$ and $\mu_e$ are the nuclear and electron magnetic moments, respectively, and $\Psi_n^2(0)$ is the density at $r=0$ of the electron in a discrete orbit. Since this doublet splitting vanishes at the ionization threshold, we transform it once again into a difference of quantum defects for the two levels. This amounts to a simple replacement of $\Psi_n^2$ by its energy-normalized counterpart $\Psi_\epsilon^2=\Psi_n^2(dn/dE)_{E=E_n}$ which yields

$$\Delta\mu=(8\pi/3I)\,\mu_N\mu_e(2I+1)\Psi_\epsilon^2(0)\,. \qquad (32)$$

For $\Psi_\epsilon^2(0)$, the $l=0$ data in Fig. 5 are fitted by the formula

$$\Psi_\epsilon^2(0)=0.88(Z^{1.035}/2\pi a^3 I_H) \qquad (33)$$

which is to be compared with the first factor of Eq. (1), namely,

$$\Psi_\epsilon^2(0)=Z/2\pi a^3 I_H\,. \qquad (34)$$

Therefore, the gross behavior of the model calculation agrees very well with the Fermi–Segrè formula. However, the large periodic fluctuations from the mean observed in Fig. 5 should be observable and should extend our understanding beyond the level of the Fermi–Segrè model. Although a large amount of data exist (Lindgren and Rosén, 1974), the comparison between the fundamental parameters discussed here and experiment is again stymied by the traditional procedure of reporting spectroscopic data for individual levels. Their reduction in terms of quantum defects and differences of quantum defects would make the properties of different levels comparable at a glance and would provide an overview of the behavior of whole Rydberg series (Fano, 1975a). A re-examination of the data of Lindgren and Rosén (1974) on this basis would be most desirable, but such a task exceeds the scope of the present paper.

For $l>0$ the strength of hyperfine interaction is proportional to the magnetic field generated by the electron at the nucleus and hence to $\langle r^{-3}\rangle$. Therefore the preceding discussion of fine structure also applies here. However it must be kept in mind that this interaction is easily overshadowed by perturbative interaction with $s$ levels which would obscure the patterns predicted by

[6] We thank Dr. M. Inokuti for pointing out to us why this particular average of $r$, unlike other weighted averages, is independent of the energy for any non-$s$ eigenstate in the pure hydrogenic field. This property arises because the centrifugal force $m^{-1}\hbar^2 l(l+1)r^{-3}$ and the Coulomb force $-Ze^2r^{-2}$ are both radial, and their algebraic sum must be equal to the time derivative of the radial component $p_r=-i\hbar r^{-1}(d/dr)r$ of the momentum. Because the average of any time derivative should vanish (the hypervirial theorem), we have $\langle m^{-1}\hbar^2 l(l+1)r^{-3}\rangle=\langle Ze^2r^{-2}\rangle$, or equivalently, $\langle r^{-2}\rangle/\langle r^{-3}\rangle=Z^{-1}l(l+1)a$, in agreement with results of explicit calculations of $\langle r^{-2}\rangle$ and $\langle r^{-3}\rangle$ [see Bethe and Salpeter, 1957, Eq. (3.25) and (3.26), p. 17].

Fig. 5.

Other phenomena which can be interpreted using the data of Fig. 5 include $\beta$ decay, inner-shell (especially $K$-shell) photoionization, internal conversion, and Auger decay, as indicated in Sec. I. Whereas we have stressed in this paper the $Z$ dependence of $\Sigma(l,Z)$ and related parameters, their energy dependence can also be treated from the same point of view. For energy ranges small compared with the strength of the potential in the region of interaction, the energy dependence of any matrix elements is totally confined to the variation in the amplitudes of energy-dependent wave functions. Consider, as an example, $K$-shell photoionization in Kr. This process consists of the ejection of an electron from the $K$ shell followed by the escape of the photoelectron to infinity. The first of these steps occurs at a mean radius of $a/Z = a/36$, where the potential is $\sim Z^2$ a.u. $\cong 30$ keV. Under these conditions the shape and nodal structure of the final state wave function in the interaction region will be independent of variations of final-state energy over a range of, say, 1% of 30 keV = 300 eV. Over this range the energy dependence of the photoionization cross section will be due solely to variations of $\alpha_1^2(0,E)$, the square of the amplitude of the outgoing $p$ wave at $r=0$. This "density of states," or "enhancement factor" as it is sometimes called, governs the escape of the photoelectron from the atomic core and therefore depends on the electron–optical properties of the weaker potential field outside the $K$ shell where energy variations of 300 eV are significant. Consequently, the energy dependence of the dipole matrix element in situations such as this can be isolated in the factor $\alpha_1^2(0,E)$ and analyzed using the PAM representation.

## VII. $Z$-DEPENDENCE OF $\delta_l$ AND $d\delta_l/dE$ AT $E=0$

The second electron–optical property we discuss is $\delta_l(E,Z)$, the phase shift of an electron in the field of a singly charged positive ion. This parameter determines the cross section for elastic scattering of electrons from the positive ions, which are found in plasmas, in the upper atmosphere, and in interstellar space. It is also relevant to the angular distribution of electrons ejected from atoms, e.g., in photoionization. Specifically, when an electron can emerge with alternative orbital momenta $(l,l')$, its angular distribution depends on the interference of the corresponding spherical harmonics $(Y_{lm},Y_{l'm'})$ and hence on the phase differences, $\delta_l - \delta_{l'}$, of their coefficients. (An additional contribution to these phase differences arises from the Coulomb field and is included in the comparison functions.) The phase shift data of Manson (1969) have been utilized extensively for this purpose (Manson, 1972). Closely related to this is the application of phase shifts to angular distributions of secondary electrons produced by charged particle impact ionization (Kim, 1972 and Madison, 1973). For electron energies below the ionization threshold, the phase shifts play the role of quantum defects in determining the energy levels of Rydberg series, through the basic formula

$$E_n = I_H/(n-\delta/\pi)^2, \quad I_H = 13.60 \text{ eV}. \tag{35}$$

In this context, the ratio $\delta/\pi$ is usually called a quantum defect and is indicated by $\mu$, as in Sec. VI, or by $\sigma$. The effect of perturbation potentials $\Delta U$, such as the spin–orbit interaction discussed in Sec. VI, is then conveniently represented by the resulting phase shift perturbation $\Delta\delta$, which yields

$$\Delta E_n = \frac{2I_H}{(n-\delta/\pi)^3}\,\frac{\Delta\delta}{\pi}, \tag{36}$$

and

$$\frac{\Delta E_n}{E_n} = \frac{2}{\pi}\left(\frac{E_n}{I_H}\right)^{1/2}\Delta\delta. \tag{36'}$$

In order to focus on the $Z$ dependence of $\delta_l$, we have evaluated this parameter at the standard energy $E=0$ for all atoms (Fig. 8). This type of plot was introduced by Manson (1969) as a part of his study of the phase shift as a function of both atomic number and energy. Equation (12) shows that, for $U \geq 0$, $\delta(r)$ is a monotonically increasing function of $r$, in contrast with $\alpha_l^2(r)$ which depends on the integration over an oscillating function in Eq. (13). As $Z$ increases, $U$ increases and additional loops of the function represented by $\sin(\phi+\delta)$ move into the core region $r < r_0$. This increase accounts for the overall upward variation of $\delta_l(r_0)$ with increasing $Z$ exhibited in Fig. 8. In addition, the variations in slope of this plot can be correlated with the nodal structure of the radial wave functions. Specifically, one can argue from

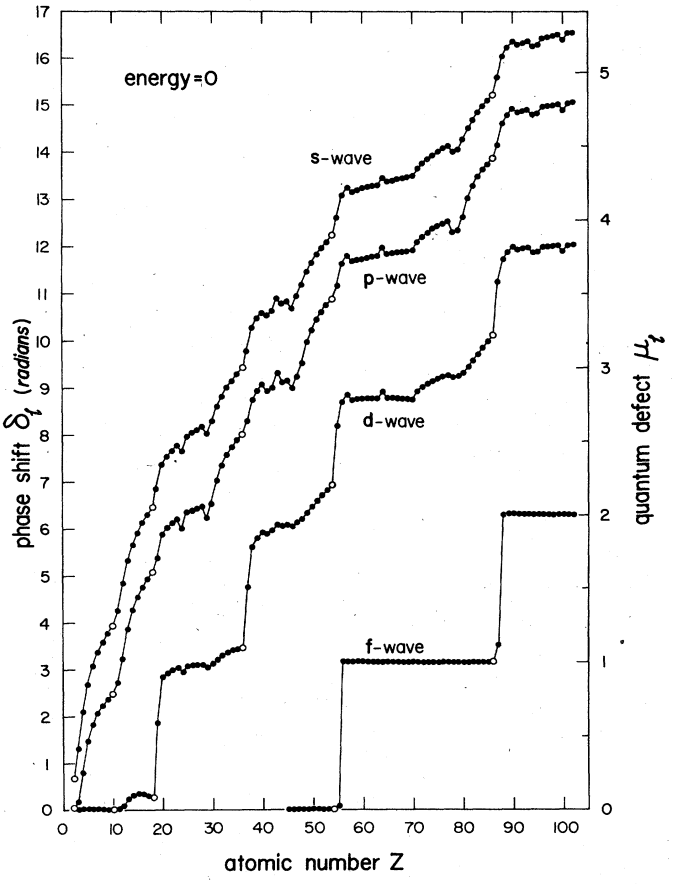


FIG. 8. Zero-energy phase shift as a function of atomic number for $l=0,1,2,3$.

Eq. (12) that $\delta_l(r_0)$ is stationary with respect to small changes $\Delta Z$ when a node occurs at $r_0$, whereas the occurrence of an antinode at $r_0$ is accompanied by large changes $\Delta\delta_l(r_0)$ over an equal range $\Delta Z$. This effect is exhibited most clearly for high $l$, where the core region of the potential, $r<r_0$, is separated from the large $r$ region by a potential barrier. This coincidence emphasizes the role of the nodal structure since the barrier occurs in the vicinity of $r_0$ and prevents a gradual transition of an antinode through this classically forbidden interval. Indeed a node occurs near $r_0$ for $l\geq 2$ over much of the Periodic System and $\delta_l(r_0)$ is accordingly stationary with $Z$, except for extremely sharp steps ($\Delta Z\sim 1$) at which one additional loop of the wave function shifts rapidly into the well inside the barrier. This behavior is also present in the plots for lower $l$, but it causes there only a modulation on a steeply rising curve as the radial nodes and antinodes pass $r_0$ more smoothly in the absence of a barrier. The derivative $d\delta_l/dE$ exhibits the effect of the nodal structure in the range $r<r_0$ more clearly as will be seen below.

This correlation between the ratio $\Delta\delta/\Delta Z$ and the location of radial nodes near $r_0$ suggests a concept which we call "mobility" of the "valence loop" of a wave function. We focus on the loop which overlaps the valence shell since the radii of the loops within the core move smoothly toward the nucleus as $Z$ increases. As in the case of $\alpha_l^2(0)$, periodic variations of $\delta_l(r_0)$ can be attributed to shifts of the valence loop which is in the process of entering into the interval $r<r_0$. Therefore, we define mobility as the change in phase shift accompanying a small increment in $Z$. Owing to the structure of Eq. (12), a large mobility corresponds to the occurrence of an antinode at $r_0$, whereas low mobility corresponds to a node at $r_0$.

This concept is illustrated both by the variation of $\delta_l$ itself and by that of the next parameter which we consider, namely, the derivative with respect to energy of the phase shift, $d\delta_l(\infty)/dE|_{E=0}$. As in the previous example, this parameter is evaluated at constant energy $E=0$, to focus on its dependence on atomic number shown in Fig. 9. Two observable dynamical properties of electrons in atomic fields depend primarily on $d\delta/dE$. One is the time delay (Wigner, 1955),

$$(\Delta t)_l = 2\hbar\, d\delta_l/dE\,, \tag{37}$$

experienced by an electron with orbital angular momentum $l$ in elastic collisions with a positive ion; more precisely this is the shift in time delay with respect to the delay in a hydrogenic field. The second application occurs in quantum defect theory, where $d\delta/dE$ relates the standard normalization of discrete eigenfunctions to a normalization per unit energy range analogous to that of continuum wave functions as follows. The square of each Rydberg state wave function normalized in the standard manner can be shown to include a factor

$$\frac{dE_n}{dn} = \left[\frac{I_H^{1/2}}{2(-E_n)^{3/2}} + \frac{1}{\pi}\left(\frac{d\delta}{dE}\right)_{E_n}\right]^{-1}. \tag{38}$$

All transition matrix elements to Rydberg states depend on $n$ through this factor, and so do the matrix elements of perturbation energies. Removal of this factor makes wave functions and matrix elements directly comparable to one another and to the corresponding quantities of the continuous spectrum.

The mobility of valence shells near the edge of the atom, i.e., at $r\sim r_0$, affects not only $\Delta\delta/\Delta Z$, but also $d\delta/dE$, since differential increments of either $Z$ or $E$ increase the effective depth of the atomic field. In the case of energy increments one should, of course, recall that the phase shifts $\delta_l$ due to the potential $U$ must generally be added to the Coulomb phase which is included in the comparison functions; this is not the case, however, either for Eq. (37) or for Eq. (38). However this consideration does not complicate our discussion significantly since the derivative of the Coulomb phase is a smooth function of $Z$.

For these reasons local maxima in the plots of Fig. 9 generally reflect a high mobility of the valence loop caused by the presence of an antinode of the wave function at $r_0$. Conversely, a local minimum denotes low mobility corresponding to the presence of a node at $r_0$. As a specific example, consider the $l=2$ waves for $20\leq Z\leq 38$. As pointed out in Sec. VI, the valence loop of a

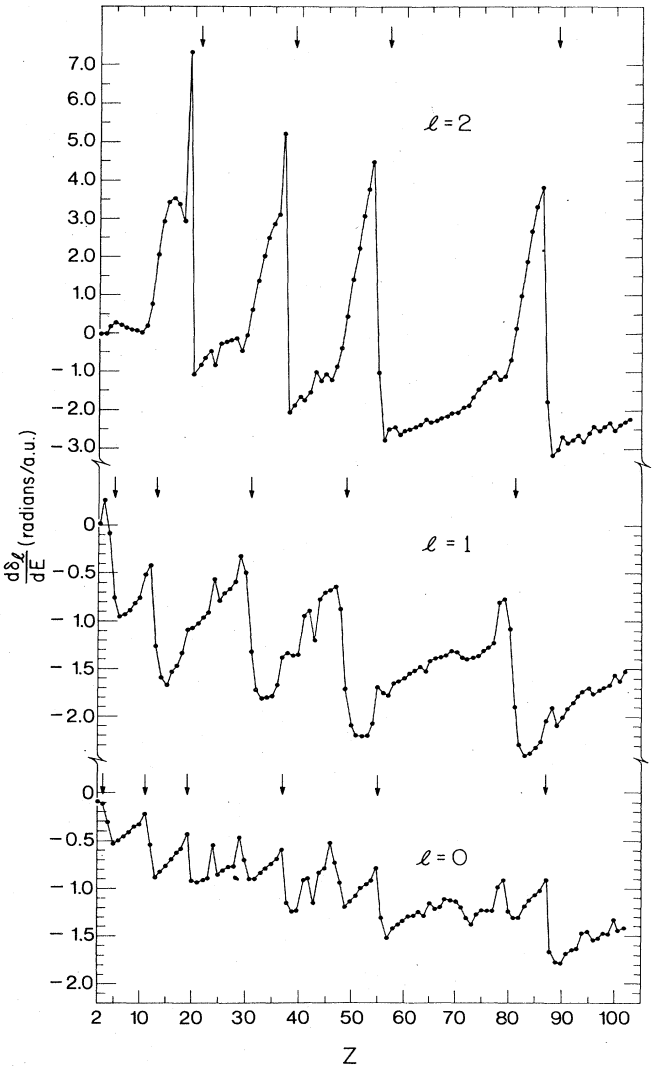


FIG. 9. Time delay parameters $d\delta_l/dE$ at $E=0$.

$d$ wave function has already shrunk into the inner well of the atomic potential one atomic number before a new $d$ subshell becomes occupied in the ground state. This is the case for the Ca atom, at which the mobility for $l=2$ has reached a minimum. This situation persists along the whole sequence of transition elements. At $Z=31$ (Ga), the next $d$ orbit begins penetrating the core as the atomic field nears the condition where it can support an additional $l=2$ loop in the inner well. The increasing slope corresponds to the penetration of the leading edge of the second loop of the $l=2$ wave function into the atomic core. At $Z=37$ (Rb), the mobility of the $d$ wave has a local maximum. This denotes the closest approach of the second $d$ antinode to $r_0$ for integer $Z$. Owing to the potential barrier, however, the passage of an antinode into the atomic core is extremely rapid, and occurs, suddenly, at noninteger $Z$. In any case, between Rb and Sr, the second $l=2$ loop moves from outside or near to $r_0$ to inside $r_0$, stabilizing $\delta_2(r_0)$ once again, and restarting the cycle.

For $l=0$, the highest mobility occurs at the alkali metals, where the valence $s$ orbital has just become occupied. (The discussion of artifacts of the model presented in Secs. III and VI becomes again relevant here.) One $Z$ later, this subshell is filled and has become relatively insensitive to small changes in the potential. At this point, attention must be transferred to the next loop in the wave function, which begins to move steadily toward $r=r_0$ as the higher $l$ subshells are filling. The mobility of this loop increases with $Z$ until it, too, becomes fully occupied, and thus stabilized against small perturbations. Many individual points deviate from this trend. These points correspond to atoms in which an electron has been transferred from the valence subshell to fill or to half-fill a $d$ or $f$ subshell.

For $p$ waves, the same pattern prevails, only it is slightly shifted in $Z$. For this case, the $d\delta/dE$ curve starts to decrease when the $p$ subshell begins to fill. This decrease continues, reaching a low plateau when the shell is half filled. After the rare gases, the values begin an upward trend as the deepening atomic well begins to attract the next loop of the $p$ wave function.

## VIII. RESPONSE OF $\alpha_l$ AND $\delta_l$ TO PERTURBATIONS LOCALIZED NEAR THE NUCLEUS

This section tests the changes of the electron–optical parameters induced by perturbations of the atomic field which are concentrated near the nucleus. That is, we shall investigate how the effects of a localized perturbation combine with those of the rest of the atomic field in modifying the amplitude and phase of an electron's wave function. As in previous sections we will concentrate on the variations of these properties along the Periodic System.

Specifically we consider the effects of two perturbations, namely: (a) a highly localized model perturbation consisting of a narrow square well (pseudo $\delta$ function) placed immediately outside the nucleus so as not to overlap it, and (b) a more physical perturbation, the kinetic energy part of the relativistic correction to the Schrödinger equation.

To distinguish the effect of these perturbations from the background of the non-Coulomb part of the atomic field we incorporate this background in our comparison functions. These functions will then be solutions of the nonrelativistic Schrödinger equation, with a HS model potential, for an electron of zero energy. As in previous sections one of the comparison functions will be the regular solution and the other will be the irregular solution which has a 90° phase lag with respect to the regular one at large $r$. Therefore these comparison functions behave at small $r$ as

$$\begin{Bmatrix} F_l \\ G_l \end{Bmatrix} \xrightarrow[r\to 0]{} \begin{Bmatrix} \propto r^{l+1} \\ \propto r^{-l} \end{Bmatrix}, \tag{39}$$

and at large $r$ as (Burgess, 1963)

$$F_l = \zeta^{-1/2}(r)\sin[\phi(r)+\delta_l], \tag{40a}$$

$$G_l = -\zeta^{-1/2}(r)\cos[\phi(r)+\delta_l]. \tag{40b}$$

The $\zeta$ and $\phi$ functions are identified by substitution in the Schrödinger equation which gives

$$\zeta^2 = k^2 + \zeta^{1/2}(d^2/dr^2)\zeta^{-1/2} \tag{41}$$

and

$$\phi(r) = \int^r \zeta(r')\,dr', \tag{42}$$

where the integration constant is fixed by the boundary condition Eq. (23) (Smith, 1971). The phase $\phi(r)$ includes the Coulomb contribution whereas $\delta_l$ is due to the non-Coulomb part of the field; the perturbation effect on the phase shift will be called $\Delta\delta_l$.

In the calculations reported here, the regular solution $F_l$ was obtained by integrating Eq. (2) by the Numerov method, taking $V$ equal to the HS model potential and starting from the small $r$ behavior of the regular Coulomb function with atomic number $Z$,[7]

$$F_l(E=0,r,Z) = \left(\frac{\pi}{2Z}\right)^{1/2}\frac{(2Zr)^{l+1}}{(2l+1)!} \times\left[1-\frac{2Zr}{(2l+2)}+\frac{(2Zr)^2}{2!(2l+2)(2l+3)}-\cdots\right] \quad \text{for } r\to 0. \tag{43}$$

The integration is extended outwards to a point beyond $r_0$ at which a standard procedure (Burgess, 1963) fits the numerical values of $F_l$ to the analytic form

$$F = A\zeta^{-1/2}(r)\sin[\phi(r)+\delta]. \tag{44}$$

The fitting yields the values of $A$ and $\delta$; normalization is achieved by replacing $F$ with $F/A$. This procedure is commonly used in single-channel photoionization calculations to normalize the final state continuum wave function and determine its phase shift [cf. Cooper (1962) and Manson and Cooper (1986)]. The value of $A$ has the same order of magnitude throughout the Periodic System because $1/A^2$ is essentially the same as the coefficient $\Sigma(l,Z)$ discussed in Sec. VI.

The irregular function $G_l$ is then obtained by integrating Eq. (2) *inwards* from large $r$, using Eq. (40b) as

[7]The relationship of atomic to Coulomb wave functions near the origin has been discussed by Pratt *et al*. (1973).

the starting behavior. The expressions (40) of $F_l$ and $G_l$ are normalized to make their Wronskian $W$ equal to unity; the constancy of $W$ was checked at each value of $r$. Through this condition, Eq. (39) is renormalized to $F_l \propto r^{l+1}/A_l$, $G_l \propto r^{-l} A_l$.

### A. Delta-function perturbation

For the purpose of probing the response of the phase and amplitude functions to highly localized perturbations of the atomic field, we chose as a standard model perturbation a square well defined by

$$\Delta U = \begin{cases} 0 & \text{for} \quad r < R_0 = 1.5\times10^{-4} \text{ a.u.} \\ V_0 = 5\times10^{5} \text{ a.u.} & \text{for} \quad R_0 \le r \le R_0 + d;\ d = 1\times10^{-3} \text{ a.u.} \\ 0 & \text{for} \quad r > R_0 + d . \end{cases} \tag{45}$$

Notice that the parameters are so chosen that $(2mV_0/\hbar^2)^{1/2} \times d = 1$; this means that in the absence of other fields the wave function would acquire a phase of 1 radian when traversing the well. In this sense the perturbation may be said to be of unit strength. The choices of $R_0$ and $d$ ensure that the well surrounds the nucleus while remaining much smaller than the $K$-shell radius for all atoms. The parameters $\Delta\delta_l$ and $\alpha_l$ are determined completely by integrations extending only over the thickness $d$ of the well as can be seen from Eqs. (6) and (8).

Figure 10 presents the values of $\Delta\delta_l(r \ge R_0 + d)$ calculated for our standard perturbation. More precisely, we have plotted $\Delta\delta_l/Z^{2l+1}$ to separate out the major effect of the unscreened Coulomb field near the nucleus upon the local amplitude of the comparison function $F_l$. This arrangement is suggested by the Born approximation formula (9), whose application to our problem yields,

$$\Delta\delta_l(r \ge R_0 + d) \cong W^{-1}(2mV_0/\hbar^2) \int_{R_0}^{R_0+d} [F_l(r)]^2\, dr . \tag{46}$$

To the extent that this approximation holds, $\Delta\delta_l$ should be approximately proportional to $[F_l(0)]^2$ and hence, according to Eqs. (43) and (24), to $Z^{2l+1}$ and to the residual factor $\Sigma(l,Z)$ plotted in Fig. 5. A comparison of Figs. 10 and 5 verifies these expectations for $l=1$ and 2. For $l=0$, however, considerable departures are observed indicating that Eq. (46) does not hold here, in agreement with the fact that $\Delta\delta_0$ is indeed of order unity for large $Z$. The magnitude of $\Delta\delta_l$ for $l \ne 0$ is extremely small, owing to the centrifugal repulsion that makes $F_l$ vanishingly small near the nucleus.

Figure 11 shows the results for the amplitude ratio $\alpha_l(0)/\alpha_l(\infty) = \alpha(R_0)/\alpha(R_0+d)$. Its departures from unity are non-negligible even for $l \ne 0$, in accordance with the Born approximation, formula (16), which in our case is

$$\frac{\alpha(0)}{\alpha(\infty)} \cong 1 - W^{-1}(2mV_0/\hbar^2) \int_{R_0}^{R_0+d} F_l(r) G_l(r)\, dr . \tag{47}$$

This expression depends on the product $F_l(r)G_l(r)$ which remains of the order unity at small $r$ where $F_l$ is very small. Indeed it follows from the renormalized small $r$ expressions, $F_l \propto r^{l+1}/A_l$, $G_l \propto r^{-l} A_l$, that the Born approximation formula (47) is independent of the normalization coefficient which alone depends on the outer shell structure of the atoms. In particular the expression (47) reduces to $(2l+1)+$(terms linear in $Z$) as $R_0 \to 0$ and $d \to 0$. Conversely, the periodic variations due the shell structure reappear for $l=0$ and medium to large $Z$ where the Born approximation fails.

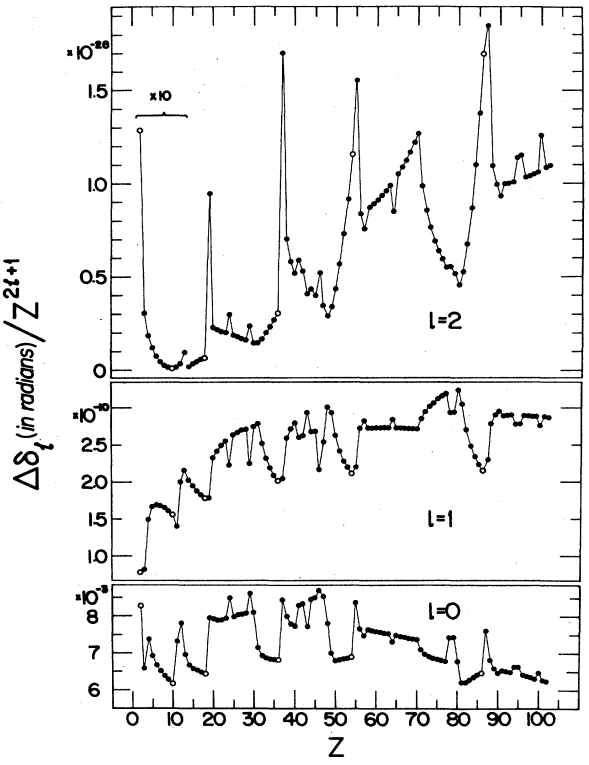


FIG. 10. Reduced values of the phase shifts induced by a square-well perturbation near the nucleus.

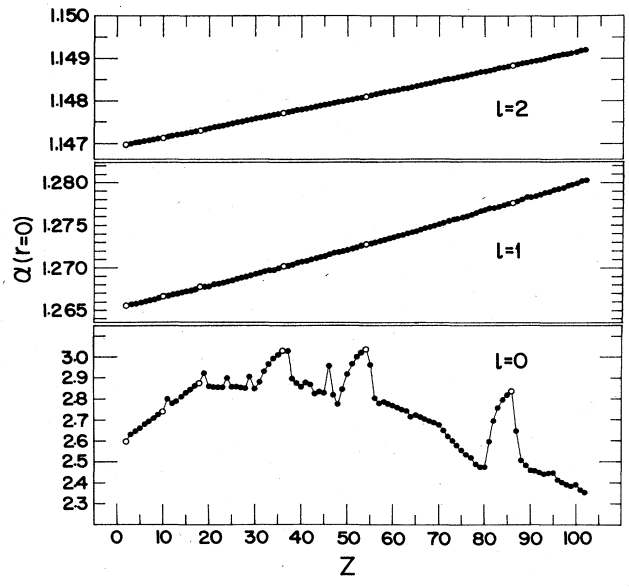


FIG. 11. Amplitude function $\alpha(r=0)$ induced by a square well perturbation near the nucleus, $\alpha(r=\infty)=1$.

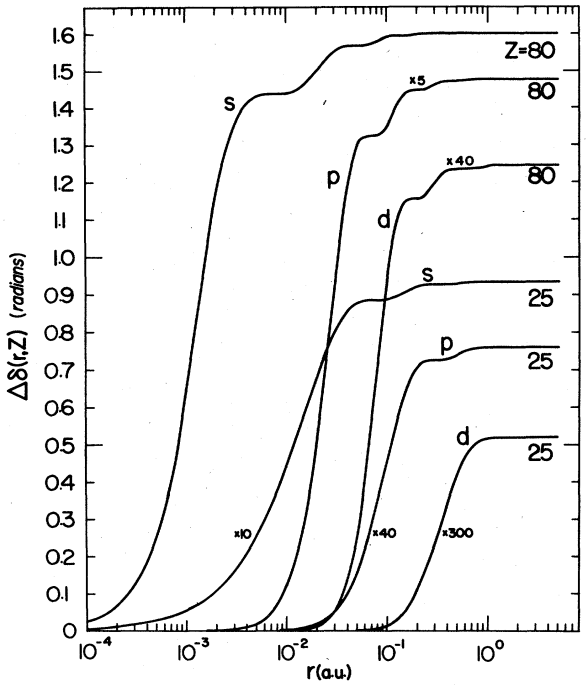


FIG. 12. Phase function correction $\Delta\delta_l(r)$ induced by the relativistic correction $\Delta U$.

## B. The relativity perturbation

In the Pauli approximation to the Dirac equation the major difference from the Schrödinger equation consists of the spherically symmetric potential field

$$\Delta U = (E - V)^2/2mc^2 . \tag{48}$$

Here $V$ represents the nonrelativistic potential, $E$ the energy—set to zero in the present application—and $\Delta U$ itself is equivalent to the $p^4/8m^3c^2$ correction to the nonrelativistic kinetic energy. The singularity of the potential $\Delta U$ which diverges as $r^{-2}$ as $r \to 0$ prevents a complete solution of the perturbed equation; however, this difficulty does not affect integration of the PAM equation for $\Delta\delta$, which proceeds outwards starting with $\Delta\delta_l = 0$ at $r = 0$.

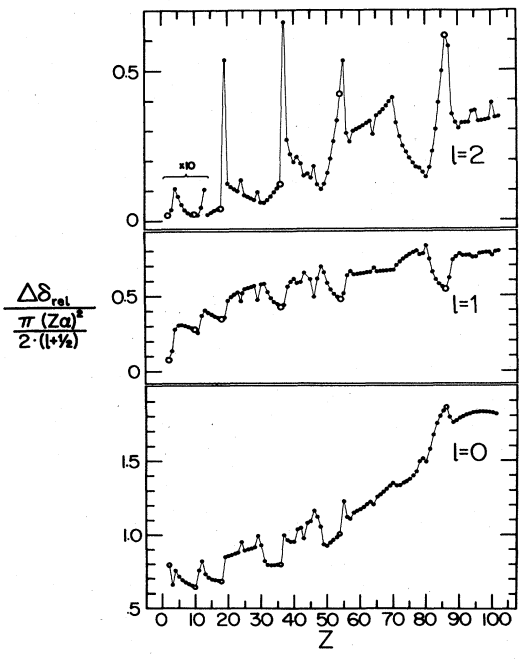


FIG. 13. Reduced values $(l+\frac{1}{2})\Delta\delta_l/\frac{1}{2}\pi Z^2\alpha^2$ of the phase shift induced by the relativistic correction $\Delta U$.

The calculation to be reported here does not constitute the solution of a realistic problem because the cumulative effects of the perturbation $\Delta U$ on *all* atomic electrons alters the electron distribution sufficiently to cause a substantial change of the initial self-consistent potential $V(r)$, quite comparable to $\Delta U$ itself. A realistic calculation should include a self-consistent readjustment of $V$ such as has been carried out by Desclaux (1973). In particular since the perturbation is attractive its main effect is to draw $s$ electrons closer to the nucleus; this initial effect increases the screening of the nuclear charge experienced by other electrons. The increased screening compensates the perturbation $\Delta U$ to some extent for $p$ electrons and even overcompensates it for the $d$ electrons which are thus, in effect, pushed out instead of being drawn in.

The main contribution of the relativistic correction should occur at small radial distances, where $\Delta U$ is largest. To illustrate this effect Fig. 12 shows the radial variation of the phase function $\Delta\delta_l(r,Z)$ for two sample values of $Z$. As expected the major rise of $\Delta\delta_l$ occurs at small values of $r$, especially for $l = 0$. Yet appreciable increases of $\Delta\delta_l(r,Z)$ are noted for values of $r > 0.1$ a.u. Stepwise increases also occur at the mean radii of the various atomic shells, where $[F_l(r)]^2$ has maxima, but these rises are much smaller, of course, than those shown in Fig. 2 since we are using here more appropriate comparison functions.

Figure 13 shows the $Z$ dependence of the terminal value reached by the phase function $\Delta\delta_l$ at $r \geq r_0$ for $l = 0$, 1 and 2. Here again we have removed the main—and smooth—part of the dependence on $Z$ by comparing $\Delta\delta_l$ to the value of $\Delta\delta_{lH}$ predicted by the hydrogenic model. That model yields a relativistic shift $\Delta E = (\alpha^2 Z^4/8n^4) \times [3 - 4n/(l+\frac{1}{2})]$ a.u. for the average of the doublet levels with quantum numbers $(n, l)$ [see, e.g., p. 60 of Bethe and Salpeter (1957)]. Conversion of this shift into a quantum defect in the limit of $n \to \infty$ (i.e., $E \to 0$), gives

$$\Delta\delta_{lH} = \pi\Delta\mu_{lH} = \tfrac{1}{2}\pi Z^2\alpha^2/(l+\tfrac{1}{2}) . \tag{49}$$

Since these values are much smaller than unity, except for heavy elements, we gather that the Born approximation formulas (9) and (10) provide a generally useful approximation, or at least a basis for qualitative analysis. Accordingly one may expect the values of $\Delta\delta_l$ to be roughly proportional to those of $[F_l(r)]^2$ near the nucleus, and hence to follow the same pattern as $[F_l(0)]^2$ in their dependence on $Z$. This expectation is generally verified by comparing Fig. 13 with Fig. 5, except for $l = 0$ and $Z > 80$, where departures from the Born approximation are quite apparent.

The calculation of the amplitude function by evaluation of the integral in Eq. (8) inwards from $r = \infty$ cannot be extended all the way to $r = 0$ owing to the divergence of $\Delta U$ which was mentioned above. However, the integral

varies smoothly as far as the smallest value of $r$ in our mesh, namely, $R_0 = 1.5\times10^{-4}$ a.u. Accordingly Fig. 14 shows the variation of $\alpha_l(R_0,Z)/\alpha_l(\infty,Z)$ or rather the ratio $[\alpha_l(R_0)/\alpha_l(\infty)-1]/Z^2$. This latter ratio is chosen because in the Born approximation the amplitude ratio departs from unity proportionally to $\Delta U$, that is, to $Z^2$. On this scale appreciable variations appear along the Periodic System comparatively large for $l=2$ where the field in the valence shells plays a larger role. These variations are an amplified manifestation of the contribution of the relativistic correction in the region of the outer shells. Here again the results agree on the whole with the Born approximation prediction except for the rapid drop of the curve for $l=0$ and $Z>80$ which reflects a lag of the relativistic effect relative to the $Z^2$ rise of the hydrogenic and Born approximations.

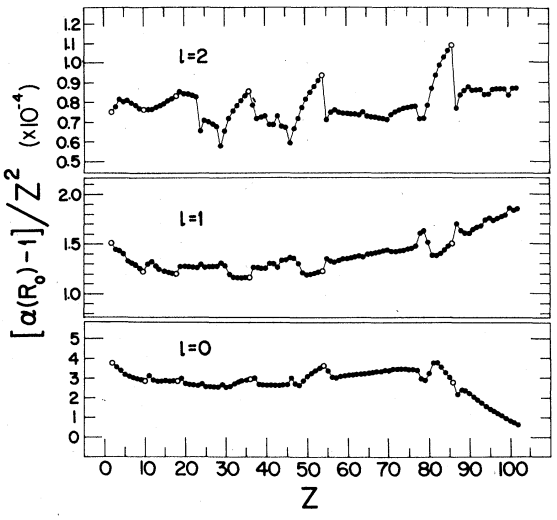


FIG. 14. Reduced values of the amplitude function $\alpha(r=R_0)$ induced by the relativistic correction $\Delta U$, evaluated at $R_0 = 1.5\times10^{-4}$ a.u., $\alpha(r=\infty)=1$.

## IX. CONCLUDING REMARKS

Both the introductory discussion in Sec. II and the display and analysis of numerical data in the body of this paper have centered on departures from hydrogenic formulas, departures attributed to inadequacy of a WKB approximation. An index of these inadequacies is afforded by the numerical parameter $\epsilon$, Eq. (18), whose magnitude has been discussed and illustrated by sample data in Sec. V. It was shown there that $\epsilon$ is far from small for electron energies near the ionization threshold. The resulting departures from WKB behavior in this energy range have been illustrated in Secs. VI–VIII.

Particularly conspicuous, in this energy range, are the effects of the centrifugal barriers which often hinder the passage of $d$ or $f$ electrons through the outer regions of atoms. The diversity of experimental manifestations of these barriers, e.g., in optical and x-ray spectra, and their critical dependence on the chemical environment of each atom have been stressed in a recent note (Fano, 1975b). Barrier effects of centrifugal or other origin are also prominent in molecular and condensed state phenomena (Dehmer, 1974; Dehmer and Dill, 1975).

On the other hand, the WKB approximation becomes increasingly appropriate as an electron's energy increases above the ionization threshold. The steady decrease of the parameter $\epsilon$ with increasing energy results from the increase of the coefficient $k_\infty^2$ in the denominator of Eq. (21). The rate of convergence of $\epsilon$ to zero over various ranges of the radial distance, for different orbital momenta and for atoms throughout the Periodic System, remains to be studied by extended calculations. However most applications of WKB-based formulas to $\beta$-decay, x-ray and Auger phenomena have probably been carried out at energies sufficiently high for $\epsilon$ to be negligible.

More specifically, the probability of $\beta$-ray emission may be evaluated as proportional to the square of a hydrogenic wave function at the nucleus, except for very low energies of escape at which the correction factor $\Sigma(l,Z)$ of Sec. VI departs appreciably from unity. Bremsstrahlung and pair production processes—for which theory summaries are given by Koch and Motz (1959) and Motz *et al.* (1969), respectively—are often localized within a distance of the order of the Compton wavelength $\lambda\!\!\!^{-}_c$ around the nucleus; this occurs typically for pair production at $\lesssim$10 MeV. In this event hydrogenic theory applies and one needs to introduce the amplitude factor $\Sigma(l,Z)$, to correct departures from WKB behavior in the outer atom, only for the escape of electrons near threshold. The importance of this effect for bremsstrahlung emission near the spectral edge has been noted above and has been illustrated by recent calculations for La using a model potential (Lee and Pratt, 1975). The localization of both bremsstrahlung and pair production spreads progressively through the whole atom at extreme relativistic energies, and for lower energy bremsstrahlung at all incident energies. Theory has taken this effect into account in the past by complementing the hydrogenic formulas by consideration of a screened potential. More recent calculations, however, have used the HS model potential instead of a hydrogenic field (Tseng and Pratt, 1971), thus including from the outset the non-WKB effects discussed in Sec. VI.

Ejection of inner-shell electrons may also result from internal conversion, photoionization or Auger effect. If a hydrogenic approximation is adequate in the region where the process occurs, the escape of the electron through the outer shells will not modify its results, except for energies near threshold at which the WKB approximation is inadequate. At such low energies, a correction is applied by multiplying the result by the coefficient $\Sigma(l,Z)$ of Sec. VI, evaluated for the appropriate escape energy and $l$ value. To improve upon the hydrogenic approximation in the relevant inner-shell region, one might utilize for the final state a wave function calculated with a realistic potential and normalized to coincide with a hydrogenic wave function near the nucleus. The approach of McEnnan *et al.* (1975) is particularly suited to this task. The calculation of this wave function need not be extended to the outer shells; its normalization may then be adjusted by multiplication of the result by $\Sigma(l,Z)$ as appropriate to take into account the escape through the outer shells.

The analysis of the fine and hyperfine interactions af-

fecting optical spectra should afford a major field of application for the points of view and results presented in this paper. However, as discussed in Sec. VI, this application has been frustrated by several circumstances. Firstly the available observational data, even though extensive, appear too fragmentary for dependable, extensive analysis of their systematic trends. Secondly, the theoretical study of these interactions has been generally conducted, thus far, on a level-by-level basis, rather by the simultaneous treatment of entire spectra which is made possible by application of quantum defect analysis (Seaton, 1966; Fano, 1975a). Finally, both the fine and hyperfine interactions decrease rapidly with increasing orbital momentum; therefore their manifestations are often distorted by perturbative coupling to lower $l$ levels, i.e., for $l$ values >1 in the case of fine structures and $l>0$ for hyperfine structures.

For elastic scattering of electrons by ions, the phase shifts can be represented as the sum of (a) the Coulomb contribution $\arg\Gamma(l+1+iz/k_\infty)$, where $z$ is the ionic charge, (b) the contribution $\delta_l$ due to the stronger field of the ionic core, which has been discussed in Sec. VII, (c) the contribution of spin–orbit coupling,

$$\Delta\delta_{lj} = \mp\{\tfrac{1}{2} \pm [1/(2l+1)]\}\,\pi\Delta\mu_l, \quad \text{for } j = l \pm \tfrac{1}{2}, \tag{50}$$

where $\Delta\mu_l$ is the parameter which was discussed in Sec. VI but should be evaluated, of course, for the appropriate value of $k_\infty \neq 0$, and (d) a relativistic correction which might be taken as the difference of relativistic and nonrelativistic hydrogenic phase shifts, $\Delta\delta_{lH}$, from Eq. (49). For high energies and low $l$, the sum of the contributions (a) and (b) is given directly by the hydrogenic value of the phase shift for the unscreened nuclear charge $Z$. Since $\Delta\delta_{lj} \ll 1$ except for the highest values of $Z$, its direct calculation using the coupling potential $r^{-1}dV/dr$ or by solving the Dirac equation should be necessary only for precision purposes. It should be recalled, however, in connection with this and all other applications, that all the considerations presented in this paper are qualified by the limitation of the model potentials, discussed in Sec. III, and particularly by the possible occurrence of inelastic processes in the traversal of an atomic field.

Relativistic effects have been explored in Sec. VIII of this paper through the evaluation of the effect of the kinetic energy correction $(E-V)^2/2mc^2$ upon the phase and amplitude functions. As noted there, this evaluation has only semi-quantitative value when applied to a single electron, because the effect under consideration modifies the whole self-consistent field of the atom. This qualification becomes unimportant for the motion of high-energy electrons, for which the WKB approximation holds outside the $K$ shell. Here, then, hydrogenic theory applies and relativistic corrections can easily be obtained by comparing the solutions of the Dirac and Schrödinger equations. Proper handling of these corrections is indeed important for applications to $\beta$-ray emission and to the hyperfine structure of $s$ and $p_{1/2}$ levels, both of which depend on the value of the wave function at the edge of the nucleus. (The exact Dirac wave function would diverge for a point nucleus.) For the emission of $\beta$ rays with $l=0$, hydrogenic theory yields a relativistic correction which rises to a factor of 10 at large $Z$ (Fano, 1952). For the hyperfine interaction the matter is more complicated because non-WKB conditions prevail near the ionization threshold throughout most of the atomic field. In this case it might be appropriate to take into account the singular behavior of the Dirac wave functions through the ratio of the Dirac–hydrogenic formula [Eq. (14.43) of Bethe and Salpeter (1957)] to the corresponding Schrödinger–hydrogenic formula; the Schrödinger $|\Psi(0)|^2$ could be evaluated separately, at the energy of interest, using a potential field based on a self-consistent relativistic calculation (Desclaux and Kim, 1975).

## ACKNOWLEDGMENT

We thank Dr. M. Inokuti and other colleagues for many discussions and advice.

## REFERENCES

Armstrong, L., 1971, *Theory of Hyperfine Structure of Free Atoms* (Wiley-Interscience, New York).
Babikov, V. V., 1967, Sov. Phys.-Usp. **92**, 271.
Babikov, V. V., 1968, *Metod phasovikh Functsii v Kvantovoi mekhanikhe* (Nauka, Moscow, USSR).
Bethe, H. A., and E. E. Salpeter, 1957, *Quantum Mechanics of One- and Two-Electron Atoms* (Springer–Verlag, Berlin, Germany).
Blatt, J. M., and V. F. Weisskopf, 1952, *Theoretical Nuclear Physics* (Wiley, New York).
Burgess, A., 1963, Proc. Phys. Soc. Lond. **81**, 442.
Calogero, F., 1967, *Variable Phase Approach to Potential Scattering* (Academic, New York).
Casimir, H. B. G., 1962, *On the Interaction Between Atomic Nuclei and Electrons* (Freeman, San Francisco).
Condo, G. T., 1974, Phys. Rev. Lett. **33**, 126.
Cooper, J. W., 1962, Phys. Rev. **128**, 681.
Cotton, F. A., and G. Wilkinson, 1967, *Advanced Inorganic Chemistry* (Interscience, New York).
Dehmer, J. L., 1973, Phys. Rev. A **7**, 4.
Dehmer, J. L., 1974, Phys. Fennica **9** S, 60.
Dehmer, J. L., and U. Fano, 1970, Phys. Rev. A **2**, 304.
Dehmer, J. L., M. Inokuti, and R. P. Saxon, 1975, Phys. Rev. A **12**, 102.
Dehmer, J. L., and D. Dill, 1975, Phys. Rev. Lett. **35**, 213.
Desclaux, J. P., 1973, At. Data Nucl. Data Tables **12**, 311.
Desclaux, J. P., and Y.-K. Kim, 1975, J. Phys. B **8**, 1177.
Fano, U., 1952, in *Tables for the Analysis of Beta Spectra* (U. S. Natl. Bur. Stand., Washington, D. C.) Appl. Math. Ser. 13.
Fano, U., 1975a, J. Opt. Soc. Am., **65**, 979.
Fano, U., 1975b, Phys. Rev. A**12**, 111.
Fano, U., and J. W. Cooper, 1968, Rev. Mod. Phys. **40**, 441.
Fano, U., and W. C. Martin, 1971, "$Z$-Dependence of Spin-Orbit Coupling" in *Topics in Modern Physics* (Colorado University Press, Boulder, Colorado), p. 147.
Fermi, E., 1934, Z. Phys. **88**, 161.
Fermi, E., 1962, Collected Papers (University of Chicago Press, Chicago).
Fermi, E., and E. Segrè, 1933, Z. Phys. **82**, 729.
Foldy, L. L., 1958, Phys. Rev. **111**, 1093.
Fröman, N., and P. O. Fröman, 1972, Phys. Rev. A **6**, 2064.
Gombás, P., 1949, *Die Statistishe Theorie des Atoms und ihre Anwendungen* (Springer–Verlag, Wien).
Griffin, D. C., K. L. Andrew, and R. D. Cowan, 1969, Phys. Rev. **177**, 62.
Hellmig, E., 1935, Z. Phys. **94**, 361.
Herman, F., and S. Skillman, 1963, *Atomic Structure Calculations* (Prentice–Hall, Englewood Cliffs, N. J.).

Inokuti, M., R. P. Saxon, and J. L. Dehmer, 1975. Int. J. Radiat. Phys. Chem. **7**, 109.
Kim, Y.-K., 1972, Phys. Rev. A **6**, 666.
Koch, H. W., and J. W. Motz, 1959, Rev. Mod. Phys. **31**, 920.
Krause, M. O., T. A. Carlson, and W. E. Moddeman, 1971, J. Phys. (Paris) **32**, C4–139.
Landé, A., 1924, Z. Phys. **25**, 46.
Landau, L. D., and E. M. Lifshitz, 1960, *Electrodynamics of Continuous Media* (Addison–Wesley, Reading, Massachusetts), p. 259, 282.
Latter, R., 1955, Phys. Rev. **99**, 510.
Lee, C. M., and R. H. Pratt, 1975, Phys. Rev. A**12**, 707.
Leon, M., and R. Seki, 1974, Phys. Rev. Lett. **32**, 132.
Lindgren, I., and A. Rosén, 1974, in *Case Studies in Atomic Physics* (North–Holland, Amsterdam), Vol. 4, p. 93.
Madison, D. H., 1973, Phys. Rev. A **8**, 2449.
Manson, S. T., 1969, Phys. Rev. **182**, 97.
Manson, S. T., 1972, J. Electron Spectrosc. **1**, 413.
Manson, S. T., and J. W. Cooper, 1968, Phys. Rev. **165**. 126.
McEnnan, J. J., and R. H. Pratt, 1975, "Analytic Perturbation Theory for Screened Coulomb Potentials: Non-Relativistic Case" Phys. Rev. to be published.
Motz, J. W., Haakon A. Olsen, and H. W. Koch, 1969, Rev. Mod. Phys. **41**, 581.
Newton, R. G., 1960, J. Math. Phys. **1**. 319.
Pratt, R. H., A. Ron, and H. K. Tseng, 1973, Rev. Mod. Phys. **45**, 273 and references therein.
Rau, A. R. P., and U. Fano, 1968, Phys. Rev. **167**, 7.
Rose, M. E., 1936, Phys. Rev. **49**. 727.
Schulz, G. J., 1973, Rev. Mod. Phys. **45**, 378.
Seaton, M. J., 1958, Mon. Not. R. Astron. Soc. **118**. 504.
Seaton, M. J., 1966, Proc. Phys. Soc. Lond. **88**, 801.
Slater, J. C., 1951, Phys. Rev. **81**, 385.
Smith, K., 1971, *The Calculation of Atomic Collision Processes* (Wiley-Interscience, New York), p. 58.
Tseng, H. K., and R. H. Pratt, 1971, Phys. Rev. A **4**, 1835.
Wiegand, C., 1969, Phys. Rev. Lett. **22**, 1235.
Wiegand, C., and G. Godfrey, 1973, Lawrence Berkeley Lab. Report No. LBL 1074, University of California, Berkeley, California.
Wigner, E. P., 1955, Phys. Rev. **98**, 145.